

# Geometry of temporal chiral structures

Andres F. Ordonez<sup>1,2</sup>, Aycke Roos<sup>3</sup>, Pablo M. Maier<sup>3</sup>, David Ayuso<sup>1,2,3</sup> and Olga Smirnova<sup>3,4</sup>

<sup>1</sup>*Department of Physics, Imperial College London, SW7 2BW London, United Kingdom*

<sup>2</sup>*Department of Chemistry, Queen Mary University of London, E1 4NS London, United Kingdom*

<sup>3</sup>*Max-Born-Institut, Max-Born-Str. 2A, 12489 Berlin, Germany*

<sup>4</sup>*Technische Universität Berlin, Straße des 17. Juni 135, 10623 Berlin, Germany*

(Dated: September 5, 2024)

arXiv:2409.02500v1 [quant-ph] 4 Sep 2024

# Abstract

In non-relativistic physics the concepts of geometry and topology are usually applied to characterise spatial structures, or structures in momentum space. We introduce the concept of temporal geometry, which encompasses the geometric and topological properties of temporal shapes, i.e. trajectories traced by a tip of a time-dependent vector in vector space. We apply it to vectors of ultrafast electron current or induced polarization in chiral molecules. The central concepts of temporal geometry – curvature and connection – emerge as ubiquitous features of photoexcited, non-equilibrium, chiral *electron* dynamics. We demonstrate that curvature and connection (i) rely on the interplay of molecular chirality and the polarization properties of light pulses, (ii) can be introduced for multiphoton processes, and (iii) control enantio-sensitive geometric observables via non-equilibrium electronic dynamics excited by tailored laser fields. Our findings may open a way to ultrafast, topologically non-trivial, and enantio-sensitive chemical dynamics.

## 1. Introduction

Synthetic chiral light [1] is an example of a locally chiral object: the Lissajous figure of its electric field vector draws a chiral three-dimensional trajectory in time at every point in space. Since its chirality is local, it can induce chiral interactions with electrons in molecules in the electric dipole approximation, promising improvement of the chiral response by orders of magnitude compared to standard methods [2] based on inefficient interactions of electrons with the magnetic field component of light. Recently, three-color locally chiral electromagnetic fields [3] have been used to harvest the electric-dipole chiral response in the microwave region [4, 5].

If the locally chiral electromagnetic field draws the same chiral Lissajous figure at every point in space in the interaction region, then the field is also globally chiral. Since different frequencies of the multicolor light combine at different points in space with different phases, such global chirality is not guaranteed *a priori*. While various set-ups can be constructed to create locally and globally chiral light [1, 6, 7], the spatial variation of the relative phases of non-collinear multicolor fields constituting locally chiral light can also be used to shape the light's handedness in space in the near field from one-dimensional patterns of alternating handedness in space [8, 9] to two-dimensional patterns forming a chiral vortex [10]. Such shaping of local handedness allows one to encode the handedness of a molecular medium in the far field emission patterns.

Locally chiral temporal structures do not have to be limited to the one traced by the tip of the light polarization vector. Electronic polarization or electronic currents induced in chiral molecules [11] can also trace temporal chiral structures. That is, the respective vectors – current or induced polarization

– trace a chiral trajectory in vector space as these vectors evolve in time. The chiral shape outlined by this trajectory is local because it is encoded in the temporal evolution of the vector, rather than in its spatial evolution. The specific chiral shape is defined by mutual orientations of the molecule and light’s polarization vector: each orientation will give rise to a different temporal chiral shape. Thus, the temporally chiral shape is defined in the configuration space of molecular orientations. If several such mutual orientations are included into the measured response, such as e.g. photoionization from the current carrying superposition of states, the set of different temporal shapes corresponding to the underlying orientations may also combine into a non-trivial global structure.

This poses several pertinent questions: (i) how is the temporal chiral geometry connected for two different orientations, and (ii) how does this connection quantify a global response for a full set of orientations? Here, we address these questions by identifying the connection and curvature associated with the *temporal geometry* of attosecond electronic response. The realization of this program requires the implementation of geometric/topological concepts into the ultrafast electronic response in chiral molecules.

While topological aspects of nuclear dynamics at conical intersections in molecules are well-known [12], the connection between topology and chirality in the light-induced electronic response of gas phase chiral molecules is an emergent topic [10, 13–16]. In these pioneering works, the respective configuration or parameter spaces range from inverse lattice vectors (in case of periodic chiral arrangement of atoms)[15] to parameters of electromagnetic waves triggering the response [14] to propagation vectors of non-linear response [10]. The desire to invoke the geometric concepts such as curvature, connection, and geometric phase is hardly surprising as it often enables one to identify novel properties of matter. Examples range from the emergence of the Fermi anti-symmetrization principle from the topology of configuration space [17], to topological materials [18, 19], anyons and topological quantum computing [20], twisted light [21], topological photonics and topological lasers [22].

The topological aspects of the *electronic* response have so far been mainly harvested in condensed matter systems and have yet to find their room in the gas and liquid phases. Since topology has an attractive property of robustness to external perturbations and noise, one may be able to create efficient and robust new enantio-sensitive observables by combining chirality and topology in the ultrafast electronic and optical response of chiral gases and liquids. Relevant experimental imperfections in gas phase experiments involve fluctuations of laser parameters, sensitivity and instrument response of photoelectron detectors, challenges in sample preparation, dilute samples and small or fluctuating enantiomeric excess in a sample. In the combination of efficiency and robustness that we are aiming

to achieve, the efficiency comes from driving an ultrafast non-linear response enabling chiral detection via electric-dipole interactions [2], whereas robustness comes from topological concepts represented locally via curvature and connection in relevant configuration or parameter spaces.

Among the first steps in this direction [10, 13–15] is a new manifestation of the Berry curvature in the *photoionization* of chiral molecules [16]. Surprisingly, it enables a new class of extremely efficient enantio-sensitive photoionization observables [16], which rely on excitation of ultrafast electronic or vibronic currents in chiral molecules, and serve as unique messengers of charge-directed reactivity [23–30]. One such observable predicts and quantifies molecular orientation dichroism in photoionization (PI-MOCD) [16]. In this case, the curvature emerges due to the geometry of the photoelectron *continuum* states. However, the Berry curvature derived in Ref. [16] is limited to adiabatic evolutions in the parameter space and one-photon ionization from a state with a stationary current.

Here we generalize our approach to extend it to (i) multiphoton processes, (ii) excitations in bound states of chiral molecules and (iii) non-adiabatic evolution. The first enables the opportunity to use tailored fields, the second opens important applications in photoexcited non-equilibrium chiral dynamics, the third removes the restriction to adiabatic evolutions of molecular degrees of freedom. We identify and describe new enantio-sensitive observables enabled by these generalizations. As a corollary of our approach, we establish the geometric origin of the photo-excitation circular dichroism (PXCD)[11] and its detection using photoionization by linearly polarized light (PXECD)[11]. Our findings establish geometrical concepts, such as the curvature<sup>1</sup> and the geometric phase, as the key quantities underlying the temporally chiral electronic response. It means that (i) there is a well-defined functional dependence of the response on these quantities, (ii) the understanding of these quantities leads to a deeply illuminating understanding of the response, (iii) those quantities can be used as effective means of detection of molecular chirality. This may open a way to generate a topologically non-trivial electronic response in photoexcited bound states of chiral molecules via tailored light fields.

The paper is organized as follows. In *Section 2* we outline the concept of *temporal geometry* in the interaction of molecules with laser pulses and present expressions for connection, curvature and vectorial and scalar observables relying on the curvature. In *Section 3* we use these expressions to provide a new general (i.e. using the connection and curvature from the outset) derivation of the geometric effect – molecular orientation by photoionization (PI-MOCD)[16]. We show that the direction of the curvature defines molecular orientation and is a direct experimental observable. This approach

---

<sup>1</sup> Since the term *Berry curvature* is reserved for adiabatic evolution in parameter space, we shall use generic notation *curvature* and *connection* for the respective geometric concepts.

shows how geometric quantities may appear in multiphoton processes, verifies our new method by comparison with the earlier results [16] and establishes the path that we follow to derive new results identifying the curvature in bound states in *Section 4* and curvature in "mixed" bound and continuum states *Section 4*. Last but not least, the efficient enantio-sensitive observables generated by *temporal geometry*, such as enantio-sensitive molecular orientation, can be controlled via excitation of non-equilibrium dynamics. In *Sections 2, 3, 6*, using the chiral molecule propylene oxide as an example, we demonstrate that simple polarization control of laser pulses allows one to switch the direction of curvature from its bound to its continuum value and thus switch the direction of enantio-sensitive orientation in PI-MOCD. Both the demonstration of the control and its fundamental understanding are new. Superscripts  $M$  and  $L$  denote that respective vectors belong to molecular or laboratory frame, respectively. Vectors contributing to scalar products will not be marked, because the pair of such vectors can be associated with any frame.

## 2. Temporal geometry in chiral molecules

Light fields  $\vec{E}(t)$  interacting with molecules primarily couple to electrons and trigger their attosecond response. In the laboratory frame <sup>2</sup> circularly polarized light interacts with randomly oriented molecules (Fig. 1(a)). Since the strength of such interaction depends on the orientation of a molecule with respect to the laser field, it inevitably couples electronic and rotational degrees of freedom. It means that the electronic current excited in molecules oriented differently will actually be different. It is easier to visualize it by switching to the molecular frame, in which the laser field would have all possible orientations (Fig. 1(b)). The coupling term now explicitly depends on the Euler angles, which characterize the orientation of the laser field in the molecular frame.

To illustrate the geometric origin of such coupling, it is convenient to associate the normal to the light polarization plane in the molecular frame with a unit radius vector on a sphere characterized by angles  $(\theta, \phi)$ . The polarization plane is tangent to this sphere. Therefore, the light's polarization vector in the molecular frame  $\vec{E}(t, \theta, \phi, \alpha)$  depends on three angles, where  $\alpha$  describes the orientation of the polarization ellipse <sup>3</sup> in the tangent plane (Fig. 1). Any change in the molecular orientation will "transport" the polarization vector along the surface of the sphere, while the electronic wave-function describing excited electrons will depend on this transport. At any point on the sphere, the laser field excites a geometrically different *temporally chiral* electronic response, because the geometry of light polarization vectors as seen by the molecule (Fig. 1(b,c)) changes from one point on the sphere

<sup>2</sup> To define the laboratory frame in the electric dipole approximation, we can not rely on the propagation vector of the laser field. Instead, we can define the laboratory frame using the two orthogonal polarization components of the laser field together with their cross product, necessitating circularly or elliptically polarized fields

<sup>3</sup> In case of circularly polarized field the angle  $\alpha$  is redundant. We omit  $\alpha$  in the following.

to another. Is there a global geometric property associated with these chiral currents for different molecular orientations?

Solving the time-dependent Schrödinger equation (TDSE) locally for each orientation characterized by a point  $\rho_0 = (\theta_0, \phi_0)$ <sup>3</sup> on the sphere of Euler angles in the electric dipole approximation:

$$i \frac{d}{dt} \psi_{el}^0(\vec{r}, \rho_0, t) = \left[ H_{el} + \vec{r} \cdot \vec{E}(\rho_0, t) \right] \psi_{el}^0(\vec{r}, \rho_0, t), \quad (1)$$

we obtain an electron wave-function  $\psi_{el}^0(t, \vec{E}(\rho_0), \vec{r})$ <sup>4</sup>, which is "agnostic" about other light field geometries. The temporally chiral shapes are generated by induced polarization  $\vec{P}(\rho, t)$  or current  $\vec{j}(\rho, t) = -\frac{\partial \vec{P}}{\partial t}$  vectors:  $\vec{P}(\rho, t) \equiv -\langle \psi_{el}^0(t, \vec{E}(\rho), \vec{r}) | \hat{r} | \psi_{el}^0(t, \vec{E}(\rho), \vec{r}) \rangle$ . Thus the question about the connection between the two currents at two different orientations reduces to the question about the connection between the two wave functions for two different  $\rho$ . Can these "local" solutions be connected in any way? Is there a curvature in the configuration space of molecular orientations, e.g. for randomly oriented molecules?

The comparison between the electron wave-function  $\psi_{el}^0(t, \vec{E}(\rho), \vec{r})$  describing the temporal geometry of chiral currents excited by the laser field fixed at a given point on the sphere  $\rho_0 = (\theta_0, \phi_0)$  with its "global" counterpart  $\psi_{el}(t, \vec{E}(\rho), \vec{r})$ , "informed" about all different laser geometries, encapsulates the essence of the "connection" between different local geometries. The TDSE for the electron wave-function  $\psi_{el}^0(t, \vec{E}(\rho_1), \vec{r})$  at some other point on the sphere has the same general form, but the laser field, of course, has a different geometry leading to a different temporally chiral response. The issue arises due to the fact that these two TDSEs are completely independent, and thus each "local" electron wave-function  $\psi_{el}^0(t, \vec{E}, \vec{r})$  is defined up to an arbitrary phase. It means that one may need to find a consistent procedure to "connect" all such solutions along a given cyclic path in the configuration space by introducing a common phase connecting all local solutions in a well-defined way and encoded in a single, consistent "full" solution  $\psi_{el}(t)$ :

$$|\psi_{el}(t)\rangle = e^{-i\alpha_D(t) + iS(t)} |\psi_{el}^0(t)\rangle. \quad (2)$$

In general, the phase has a dynamical  $\alpha_D(t)$

$$\alpha_D(t) = \int_0^t d\tau \langle \psi_{el}(\tau) | H(\tau) | \psi_{el}(\tau) \rangle, \quad (3)$$

<sup>4</sup> For simplicity we consider a single electron problem.

and a geometric  $S(t)$

$$S(t) = i \int_0^t d\tau \langle \psi_{\text{el}}^0(\tau) | \frac{\partial}{\partial \tau} | \psi_{\text{el}}^0(\tau) \rangle \quad (4)$$

components. Our "local" solution  $\psi_{\text{el}}^0(t)$  is known as a *closed lift* of a state vector defined as  $|\psi_{\text{el}}(t)\rangle \langle \psi_{\text{el}}(t)|$  (see [31] and Appendix A). In Appendix B we show that, in the case of a periodic evolution of  $\vec{E}(t, \rho)$  in the space of Euler angles, the connection is a vector potential

$$\vec{A}(\vec{E}) = i \langle \psi_{\text{el}}^0(\vec{E}) | \vec{\nabla}_{\vec{E}} \psi_{\text{el}}^0(\vec{E}) \rangle, \quad (5)$$

quantifying the change in the local wave-function in response to the change in the laser field geometry. It specifies the geometric phase  $S$  accumulated after a full cycle of evolution of  $\vec{E}(t, \rho)$  in the space of Euler angles  $\rho$  as detailed in Appendix B:

$$S = \oint i \langle \psi_{\text{el}}^0(\vec{E}) | \vec{\nabla}_{\vec{E}} \psi_{\text{el}}^0(\vec{E}) \rangle d\vec{E} = \oint \vec{A}(\vec{E}) \cdot d\vec{E}. \quad (6)$$

This connection leads to the geometric magnetic field (the curvature):

$$\vec{\Omega} = \vec{\nabla}_{\vec{E}} \times \vec{A} = i \langle \vec{\nabla}_{\vec{E}} \psi_{\text{el}}^0(\vec{E}) | \times | \vec{\nabla}_{\vec{E}} \psi_{\text{el}}^0(\vec{E}) \rangle. \quad (7)$$

Eqs. (5,7) encapsulate the origin of the geometric magnetism, emerging due to the necessity to "connect" *temporal geometry* at different points in configuration space. Eqs. (5,7) emphasize the dynamical, laser-driven origin of these geometric quantities. As derived, Eqs. (5,7) appear general and applicable to any light-driven process.

In the next sections, we test the generality of Eq. (7) by applying it to three different types of two-photon processes involving linearly and circularly polarized pump and probe pulses. First, we generalize the relationship between the curvature (Eq. (7)) and the vectorial observables expressing the light-induced enantio-sensitive molecular orientation by ionization of an initially randomly oriented ensemble of molecules, extending our earlier work [16], where we derived the curvature for one-photon ionization from a state with a stationary current. Second, we identify new observables describing enantio-sensitive orientation by excitation, opening new opportunities for controlling the direction of orientation. Third, we derive the relationship between the photoionization yield and the curvature Eq. (7) in two-photon ionization by circularly polarized field. We show that it is similar to

the one in one-photon ionization from a state with a stationary current [16], confirming the generality of the link between the enantio-sensitive photoionization yield and the geometric phase.

Specifically, we show that enantio-sensitive molecular orientation can be expressed using Eq. (7) as follows (superscripts  $L$  and  $M$  stand for laboratory and molecular frame correspondingly):

$$\langle \vec{e}_\Omega^L \rangle = \sigma \left\langle \left( \vec{\Omega}^L \cdot \hat{z}^L \right) \vec{e}_\Omega^L \right\rangle = \sigma \mathbf{R}^{(n,p)} \langle \vec{\Omega}^M \cdot \vec{e}_\Omega^M \rangle \hat{z}^L. \quad (8)$$

Here  $\langle \vec{e}_\Omega^L \rangle$  is the orientationally averaged value of a unit vector directed along the curvature in the molecular frame ( $\vec{e}_\Omega^M \parallel \vec{\Omega}^M$ ),  $\sigma = \pm 1$  is the direction of rotation of the light field,  $\langle \vec{\Omega}^M \cdot \vec{e}_\Omega^M \rangle$  is the orientationally averaged value of a scalar product  $\vec{\Omega}^M \cdot \vec{e}_\Omega^M$ ,  $\mathbf{R}^{(n,p)}$  is a factor associated with the partial alignment of the molecular ensemble due to excitation or ionization, which depends on the number of absorbed photons  $n$ . Superscript  $p$  in  $\mathbf{R}^{(n,p)}$  indicates that it also depends on polarizations of absorbed photons, which may or may not break the cylindrical symmetry of the set-up. We establish the factor  $\mathbf{R}^{(n,p)}$  by explicitly evaluating  $\left\langle \left( \vec{\Omega}^L \cdot \hat{z}^L \right) \vec{e}_\Omega^L \right\rangle$  and  $\langle \vec{\Omega}^M \cdot \vec{e}_\Omega^M \rangle$  using Eq. (7).

Eq. (8) shows that (i) the vector  $\langle \vec{e}_\Omega^L \rangle$  orients itself along the direction of photon spin  $\hat{z}^L$ , and (ii) the curvature controls the direction and the degree of molecular orientation. To demonstrate the generality of our approach, we use Eqs. (7,8) to evaluate enantio-sensitive molecular orientation for a range of two-photon processes and compare the resulting expressions with the direct evaluation, where the curvature is not employed. We show that the results are equivalent. Our approach not only allows us to express enantio-sensitive molecular orientation in a compact way (Eq. (8)), but also uncovers its fundamental origin, appearing to be invariant for different multiphoton processes.

Moreover, we also show that the enantio-sensitive and dichroic part of photoionization yield in a two photon process for an oriented molecule is proportional to the projection of the curvature on the light propagation axis:

$$W_\sigma(\rho) - W_{-\sigma}(\rho) = \sigma \left( \vec{\Omega}_\sigma^L(\rho) + \vec{\Omega}_{-\sigma}^L(\rho) \right) \cdot \hat{z}^L. \quad (9)$$

This expression is essentially the same as in the one-photon case [16], leading to a similar relationship between the total, i.e. orientationally averaged yield, and the geometric phase in the multiphoton regime for circularly polarized pulses:

$$W_\sigma - W_{-\sigma} = \int d\rho W_\sigma(\rho) - W_{-\sigma}(\rho) = \frac{\sigma}{4\pi} \int \left( \vec{\Omega}_\sigma^M(k, \theta, \phi) + \vec{\Omega}_{-\sigma}^M(k, \theta, \phi) \right) \cdot d\vec{S}^M = \frac{\sigma}{4\pi} \left( \Phi_\sigma^{ES} + \Phi_{-\sigma}^{ES} \right). \quad (10)$$

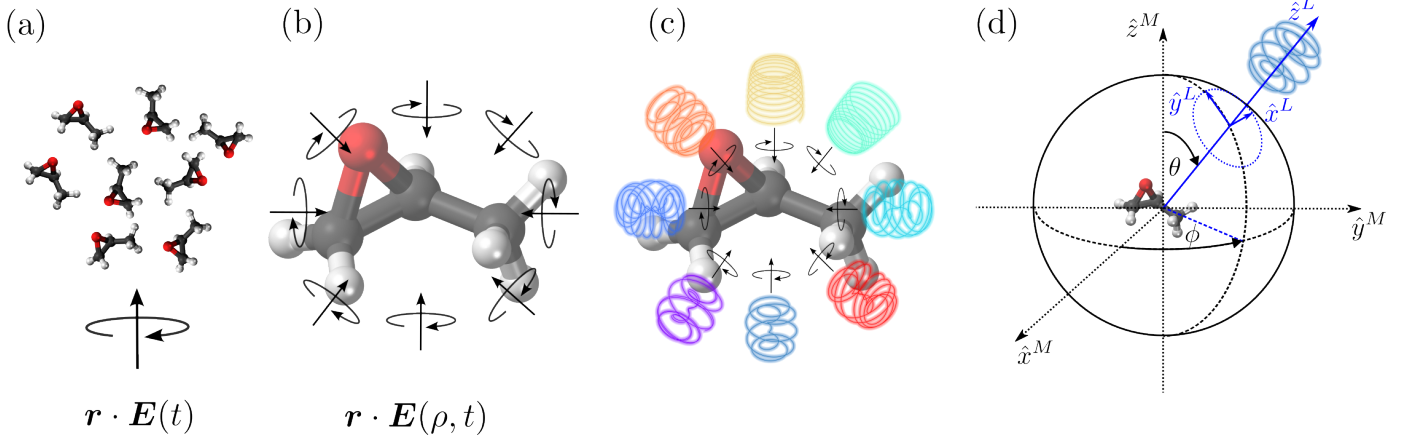


**Figure 1** The idea of temporal geometry. Panel (a) shows structured light incident on an ensemble of randomly oriented molecules in the laboratory frame. In the molecular frame (panel (b)), the molecule is fixed, so it is the light that changes its orientation. Depending on the orientation, different chiral electronic currents can be induced. They are represented by glowing curves in panel (c). Panel (d): The molecular frame is defined by axes:  $\hat{x}^M$ ,  $\hat{y}^M$ ,  $\hat{z}^M$ . The laboratory frame is defined by the polarization plane  $\hat{x}^L$ ,  $\hat{y}^L$  and the light propagation vector  $\hat{z}^L$ . The polarization plane is tangent to the sphere at the points  $(\theta, \phi)$ . The third angle  $\alpha$  (not shown) defines the orientation of the polarization ellipse. The blue curve represents a chiral 3D shape drawn by electronic current excited by the laser field polarization in the plane tangent to the sphere in points  $(\theta, \phi)$ .

Here  $\int d\vec{S}^M = \vec{e}_r^M \int_0^\pi \sin \theta d\theta \int_0^{2\pi} d\phi$ , where  $\vec{e}_r^M$  is a unit radial vector in the molecular frame, corresponding to the orientation of the photon spin in the molecular frame, the third Euler angle  $\alpha$  (Fig. 1(d)) is not relevant for circularly polarized pulses. First, Eq. (10) shows that the enantio-sensitive yield is proportional to the orientationally averaged radial component of the curvatures  $\langle \Omega_{r,\sigma}^M(k) \rangle + \langle \Omega_{r,-\sigma}^M(k) \rangle$ . Second, Eq. (10) expresses the flux of the curvature (for a given  $\sigma$ ) through the parameter space of field orientations (Fig. 1(d)), which by definition is equal to the geometric phase  $\Phi_\sigma^{ES}$ . The superscript *ES* emphasizes the enantio-sensitive nature of the geometric phase.

### 3. Temporal geometry in two-photon ionization

We can use Eq. (7) to calculate the curvature for a two-photon process, in which a linearly polarized pulse excites a superposition of states in a molecule and a circularly polarized pulse photoionizes this superposition. Since only spin carrying light fields induce temporal geometry, we use a linearly polarized pulse to excite the molecule to separate the curvature due to the continuum states from the curvature due to the bound states (see Section 4). If excitation and ionization are performed with the same circularly polarized pulse, then the contributions of the bound and continuum states to the curvature are mixed (see Section 5).

We use perturbation theory to calculate  $|\psi(\vec{E})\rangle$  explicitly:

$$\psi = \psi_0 + a_1 \psi_1 + a_2 \psi_2 + \int d\Theta_k a_{\vec{k}} \psi_{\vec{k}}. \quad (11)$$

Here  $d\Theta_k = \sin \theta_k d\theta_k d\phi_k$  and  $\theta_k, \phi_k$  are angles characterizing the direction of the photoelectron momentum  $\vec{k}$  for fixed  $k = |\vec{k}|$ ,  $a_i$  and  $a_{\vec{k}}$  are the amplitudes of bound ( $i = 1, 2$ ) and continuum states:

$$a_i = i \int_0^t dt' \vec{d}_i \cdot \vec{\mathcal{E}}_i(t') e^{i\omega_i t'} = i \vec{d}_i \cdot \vec{\mathcal{E}}_i, \quad (12)$$

$$a_{\vec{k}} = - \left( \vec{D}_1 \cdot \vec{E}_{\vec{k}1} \right) \left( \vec{d}_1 \cdot \vec{\mathcal{E}}_1 \right) e^{-i\omega_1 \tau} - \left( \vec{D}_2 \cdot \vec{E}_{\vec{k}2} \right) \left( \vec{d}_2 \cdot \vec{\mathcal{E}}_2 \right) e^{-i\omega_2 \tau}. \quad (13)$$

Here  $\vec{d}_i$  are bound transition dipoles, and  $\vec{D}_i$  are photoionization dipoles from bound states ( $i = 1, 2$ ) to the continuum state  $\vec{k}$ . Writing  $\vec{E}_{\vec{k}i} = |E_{\omega_{\vec{k}i}}| \vec{E}$ , with  $\vec{E} = \frac{1}{\sqrt{2}} (\hat{x} + i\sigma\hat{y})$  and taking the space spanned by the probe polarization  $\vec{E}$  as the parameter space as suggested by Eq. (7), the curvature (Eq. (7)) in the molecular frame yield

$$\vec{\Omega}_{\text{ion}}^M(k, \rho) = -|E_{\omega_{\vec{k}1}}| |E_{\omega_{\vec{k}2}}| \text{Im} \left\{ \left( \vec{d}_1 \cdot \vec{\mathcal{E}}_1 \right)^* \left( \vec{d}_2 \cdot \vec{\mathcal{E}}_2 \right) e^{i\omega_{12}\tau} \int d\Theta_k \vec{D}_1^{*M} \times \vec{D}_2^M \right\} \quad (14)$$

where the subscript 'ion' emphasizes that the curvature  $\vec{\Omega}_{\text{ion}}^M(k, \rho)$  relies on the continuum states and manifests itself in photoionization. The superscript  $M$  emphasizes that vectors are expressed in the molecular frame. The direction of the curvature in the molecular frame is defined by the direction of the vector  $\vec{P}_{12}^{+M}(k)$ , where  $\vec{P}_{12}^{+M}(k) \equiv \frac{1}{2} \text{Im} \left\{ i \int d\Theta_k \vec{D}_1^{*M} \times \vec{D}_2^M \right\}$ , superscript "+" indicates that only  $\vec{k}$ -even part of the vector product contributes to the integrated quantity (see also [16]).

We now introduce the polar unit vector  $\vec{e}_{\Omega}^M$  along the direction of the curvature  $\vec{\Omega}_{\text{ion}}^M(k, \rho)$  (i.e. along  $\vec{P}_{12}^{+M}(k)$ ) and obtain the averaged value of  $\langle \vec{\Omega}_{\text{ion}} \cdot \vec{e}_{\Omega} \rangle$ <sup>5</sup> (see Appendix D):

$$\langle \vec{\Omega}_{\text{ion}}(k) \cdot \vec{e}_{\Omega} \rangle = -\frac{1}{3} C \left( \vec{d}_1 \cdot \vec{d}_2 \right) \left( \vec{P}_{12}^+(k) \cdot \vec{e}_{\Omega} \right) \sin(\omega_{12}\tau) = -\frac{1}{3} v C \left( \vec{d}_1 \cdot \vec{d}_2 \right) |\vec{P}_{12}^+(k)| \sin(\omega_{12}\tau), \quad (15)$$

where  $C \equiv |E_{\omega_{\vec{k}1}}| |\mathcal{E}_{\omega_1}| |E_{\omega_{\vec{k}2}}| |\mathcal{E}_{\omega_2}|$ . Note that  $\vec{P}_{12}^+(k) \cdot \vec{e}_{\Omega} = v |\vec{P}_{12}^+(k)|$ , where  $v = \pm 1$  is molecular pseudoscalar. The enantio-sensitive molecular orientation by ionization (PI-MOCD) for the linear pump - circular probe excitation is associated with the preferential photoionization of the molecules with the curvature oriented along the photon spin. Using Eq. (8) together with Eq. (14) we can calculate (see

<sup>5</sup> Here and in the following we omit indices  $M, L$  in scalar products, since the scalar products are rotationally invariant and can be associated with any frame.

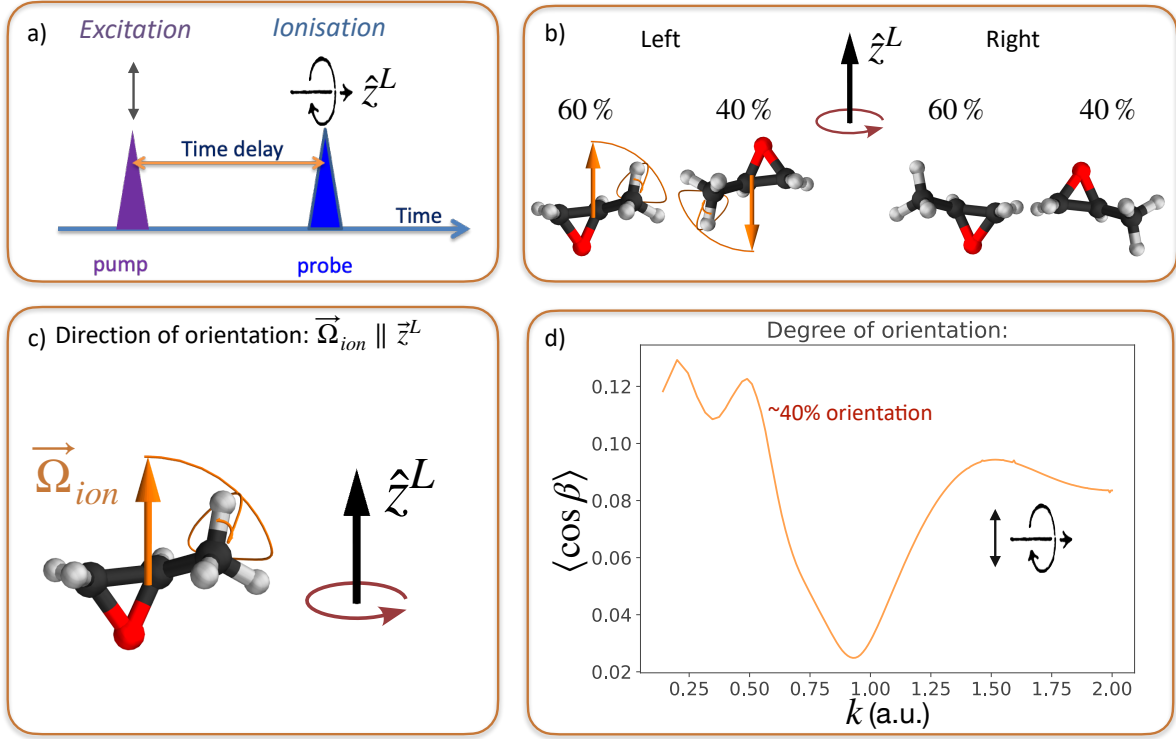


**Figure 2** Enantio-sensitive molecular orientation by photoionization. (a) Linearly polarized pump pulse excites the superposition of LUMO and LUMO<sub>+1</sub> states in propylene oxide, circularly polarized probe ( $\hat{z}^L$  is the direction of photon spin in the laboratory frame) removes the excited electron. (b) Molecules with the curvature  $\vec{\Omega}_{ion} \parallel \hat{z}^L$  are preferentially ionized, leading to enantio-sensitive delay dependent orientation of cations.  $\vec{\Omega}_{ion}$  depends on the excited superposition and photoelectron energy. As a function of photoelectron energy, the tip of the curvature vector traces the orange curve in space. This orange curve illustrates the sequence of orientations achieved for different final photoelectron momenta, from 0.25 to 2 a.u. Estimated percentages of "up" and "down" oriented species correspond to the maximal value of  $\langle \cos \beta \rangle \simeq 0.11$  and obtained using the same model as in Ref. [16]. (c) Direction of molecular orientation is defined by the curvature vector. (d) Expectation value  $\langle \cos \beta \rangle$  as a function of photoelectron momentum  $k$  (in atomic units). The values have been taken at the time-delay that maximizes  $\langle \hat{e}_{\Omega}^L \rangle$  and have been normalized to the total yield averaged over the pump-probe time delay

Appendix D) the orientation averaged value of  $\langle \hat{e}_{\Omega}^L \rangle$ :

$$\langle \hat{e}_{\Omega}^L \rangle_{\uparrow, \circ} = \sigma \left\langle \left( \vec{\Omega}_{ion}^L \cdot \hat{z}^L \right) \hat{e}_{\Omega}^L \right\rangle = \sigma R^{(2, \uparrow, \circ)} \langle \vec{\Omega}_{ion} \cdot \vec{e}_{\Omega} \rangle \hat{z}^L, \quad (16)$$

where

$$R^{(2, \uparrow, \circ)} \equiv \frac{2}{5} \left[ 1 - \frac{1}{2} \frac{(\vec{d}_1 \cdot \vec{E})(\vec{d}_2 \cdot \vec{e}_{\Omega})}{(\vec{d}_1 \cdot \vec{d}_2)} \right]. \quad (17)$$

Up to notations Eq. (16) reproduces our earlier result for PI-MOCD [16], validating the general approach (i.e. calculating  $\langle \hat{e}_{\Omega}^L \rangle$  using Eqs. (7 and 8) developed here. Vector  $\langle \hat{e}_{\Omega}^L \rangle$  can be used to find the

expectation value of  $\cos\beta$ , where  $\beta$  is the angle between the unit vector along the curvature  $\vec{e}_\Omega^L$  and the direction of photon spin. The value of  $\cos\beta$  (see Fig. 2(c)) is given by the normalized (to the total photoionization yield averaged over the pump-probe delay) magnitude of  $\langle \vec{e}_\Omega^L \rangle$ .

#### 4. Temporal geometry in photoexcitation

The curvature can also be associated with the excitation of bound states. Importantly, the general definition Eq. (7) describes both cases, even though the specific expressions are different. This surprising result demonstrates the importance of laser pulse polarization geometry: applying a circularly polarized pulse either to photoionize or to excite the molecule, one can address these two different "faces" of the curvature.

Let a circularly polarized pump pulse excite a superposition of states in a chiral molecule. We now show that the subsequent photoionization by a linearly polarized probe pulse will lead to enantio-sensitive orientation of ions (PI-MOCD). Exchanging  $\vec{E}_{ki}$  and  $\vec{e}_i$  in Eq. (13), using Eq. (7) and following the same steps as in the previous section we obtain the analog of Eq. (14):

$$\vec{\Omega}_{\text{exc}}^M(k, \rho) = -|E_{\omega_1}| |E_{\omega_2}| \text{Im} \left\{ \int d\Theta_k \left( \vec{D}_1 \cdot \vec{e}_{k1} \right)^* \left( \vec{D}_2 \cdot \vec{e}_{k2} \right) e^{i\omega_{12}\tau} \right\} \left( \vec{d}_1^M \times \vec{d}_2^M \right). \quad (18)$$

Here the subscript 'bound' emphasizes the nature of the curvature, which now relies on bound states.

The orientationally averaged expression for the scalar product  $\vec{\Omega} \cdot \vec{e}_\Omega$ , where  $\vec{e}_\Omega$  is oriented along the direction of  $(\vec{d}_1 \times \vec{d}_2)$  in the molecular frame, can be derived in the same way as in the previous section:

$$\langle \vec{\Omega}_{\text{exc}}(k) \cdot \vec{e}_\Omega \rangle = -\frac{1}{3} C \text{Re} \left\{ \int d\Theta_k \vec{D}_1^* \cdot \vec{D}_2 \right\} \left( \vec{d}_1 \times \vec{d}_2 \right) \cdot \vec{e}_\Omega \sin(\omega_{12}\tau), \quad (19)$$

where  $C \equiv |\mathcal{E}_{\omega_{k1}}| |E_{\omega_1}| |\mathcal{E}_{\omega_{k2}}| |E_{\omega_2}|$  and we took into account that for the time-reversal-invariant excited states  $\psi_1$  and  $\psi_2$ , the time-reversal symmetry implies that (see Appendix C):

$$\text{Im} \left\{ \int d\Theta_k \vec{D}_1^* \cdot \vec{D}_2 \right\} = 0. \quad (20)$$

Note that  $(\vec{d}_1 \times \vec{d}_2) \cdot \vec{e}_\Omega = v \left| \vec{d}_1 \times \vec{d}_2 \right| \vec{e}_\Omega$ , meaning that Eq. (19) can also be rewritten as

$$\langle \vec{\Omega}_{\text{exc}}(k) \cdot \vec{e}_\Omega \rangle = -\frac{1}{3} v C \text{Re} \left\{ \int d\Theta_k \vec{D}_1^* \cdot \vec{D}_2 \right\} \left| \vec{d}_1 \times \vec{d}_2 \right| \sin(\omega_{12}\tau). \quad (21)$$

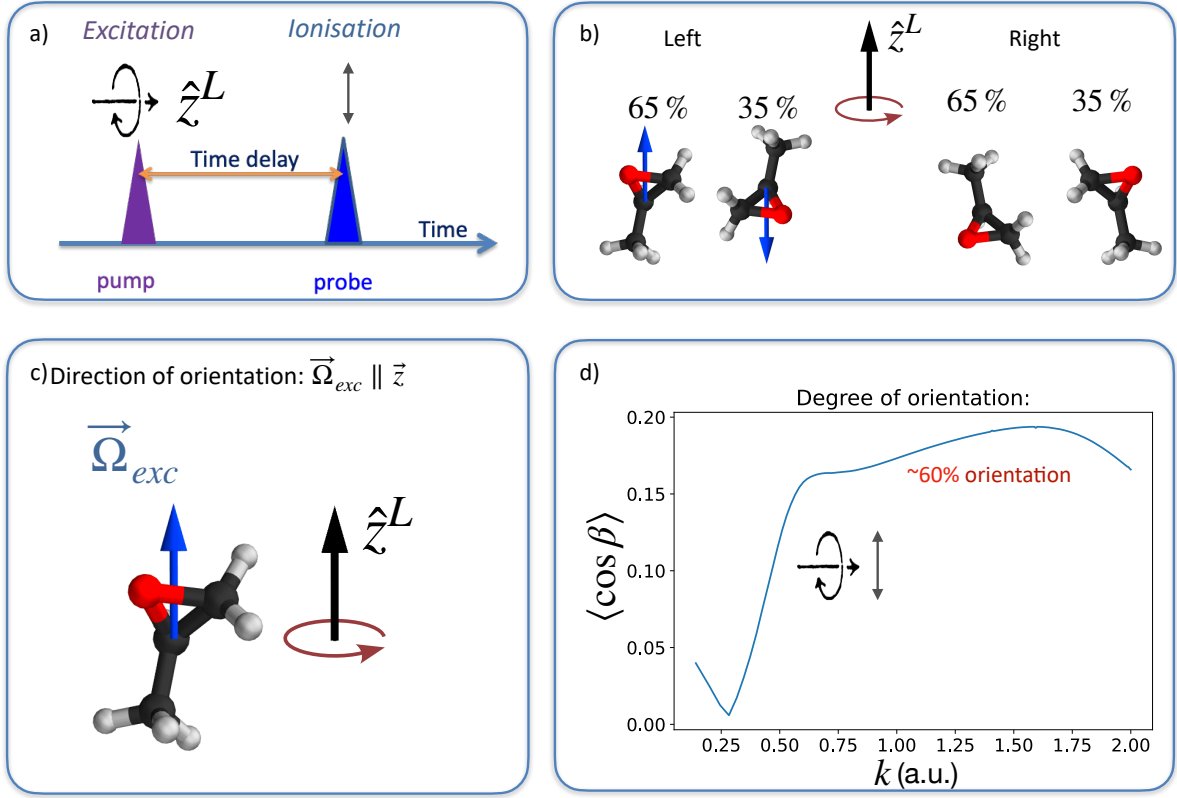


**Figure 3** Enantio-sensitive molecular orientation by excitation probed via photoionization. (a) Circularly polarized pulse ( $\hat{z}^L$  is the direction of photon spin in the laboratory frame) excites a superposition of LUMO and LUMO<sub>+1</sub> states in propylene oxide. (b) Molecules with  $\vec{\Omega}_{exc} \parallel \hat{z}^L$  are excited preferentially. A linearly polarized probe removes the excited electron, leading to enantio-sensitive delay dependent orientation of cations. Estimated percentages of "up" and "down" oriented species correspond to the maximal value of  $\langle \cos \beta \rangle \simeq 0.19$  and are obtained using the same model as in Ref. [16] (c) Direction of molecular orientation is defined by the curvature vector. (d) Expectation value  $\langle \cos \beta \rangle$  as a function of photoelectron momentum  $k$  (in atomic units). The values have been taken at the time-delay that maximizes  $\langle \hat{z}^L \rangle$  and have been normalized to the total yield averaged over the pump-probe time delay.

Using Eq. (8) together with Eq. (18) we can calculate (see Appendix D) the orientation averaged value of

$$\langle \hat{e}_{\Omega}^L \rangle^{\circ, \uparrow} = \sigma \left\langle \left( \vec{\Omega}_{exc}^L \cdot \hat{z}^L \right) \hat{e}_{\Omega}^L \right\rangle = \sigma R^{(2, \circ, \uparrow)} \langle \vec{\Omega}_{exc} \cdot \vec{e}_{\Omega} \rangle \hat{z}^L, \quad (22)$$

where

$$R^{(2, \circ, \uparrow)} \equiv \frac{2}{5} \left[ 1 - \frac{1}{2} \frac{Re \left\{ \int d\Theta_k (\vec{D}_1^* \cdot \vec{E}) (\vec{D}_2 \cdot \vec{e}_{\Omega}) \right\}}{Re \left\{ \int d\Theta_k (\vec{D}_1^* \cdot \vec{D}_2) \right\}} \right]. \quad (23)$$

Evaluating it explicitly

$$\langle \vec{e}_\Omega^L \rangle^{\circ, \uparrow} = \int d\rho W^{\uparrow, \circ}(k, \rho) \vec{e}_\Omega^L, \quad (24)$$

we get the expression equivalent to Eq. (22), up to rearrangement of terms:

$$\langle \vec{e}_\Omega^L \rangle^{\circ, \uparrow} = \frac{i\sigma}{60} C \int d\Theta_k \left[ 4 \left( \vec{D}_2^* \cdot \vec{D}_1 \right) \vec{e}_\Omega^M - \left( \vec{D}_2^* \cdot \vec{e}_\Omega \right) \vec{D}_1^M - \left( \vec{D}_1 \cdot \vec{e}_\Omega \right) \vec{D}_2^{*M} \right] \left( \vec{d}_2^M \times \vec{d}_1^M \right) e^{i\omega_{21}t \hat{z}} + \text{c.c.} \quad (25)$$

Eq. (22) together with Eq. (19) show that PI-MOCD can also emerge due to curvature in bound states: molecules, in which the curvature is oriented along the spin of the laser light, are excited preferentially. Thus, photoionization following photoexcitation creates enantio-sensitive orientation of both neutrals and cations. The expectation value of  $\cos \beta$ , where  $\beta$  is the angle between the unit vector along the curvature  $\vec{e}_\Omega^L$  and the direction of photon spin, is given by the normalized (to the total photoionization yield averaged over the pump-probe delay) magnitude of  $\langle \vec{e}_\Omega^L \rangle$ .

## 5. Interplay of bound and continuum temporal geometries

In the previous two sections, we considered photoexcitation followed by photoionization induced by pairs of pump-probe pulses with linear - circular or circular-linear polarizations correspondingly. In the first case, the curvature has emerged due to the temporal geometry in photoelectron continuum states, in the second case it has emerged due to the temporal geometry in bound states. What happens if both the pump and the probe pulses are circularly polarized?

To answer this question, we need to apply Eqs. (7) to equations (11-13), where the Fourier components of linearly polarized fields  $\vec{\mathcal{E}}_2$  and  $\vec{\mathcal{E}}_1$  are substituted by the Fourier components of circularly polarized fields:  $\vec{\mathcal{E}}_2 \Rightarrow \vec{E}_2$  and  $\vec{\mathcal{E}}_1 \Rightarrow \vec{E}_1$ . Note that there is a difference in using Eq. (7) in this case. As detailed in Appendix B, the gradients  $\vec{\nabla}_{\vec{E}}$  in Eq. (7) should be taken only with respect to fields carrying spin angular momentum, because only these fields uniquely define the orientation of the laboratory frame with respect to the molecular frame. That is why in sections 3,4 the gradients  $\vec{\nabla}_{\vec{E}}$  were taken only with respect to the circularly polarised Fourier components of the field (i.e. probe field in Section 3 and pump field in Section 4). Here, we have to evaluate the gradients with respect to both the pump field components and the probe field components. It leads to the following expression for the curvature (see Appendix F):

$$\vec{\Omega}^M(k, \rho) = \vec{\Omega}_{\text{exc}}^M(k, \rho) + \vec{\Omega}_{\text{ion}}^M(k, \rho) + \vec{\Omega}_{\text{mix}}^M(k, \rho) \quad (26)$$

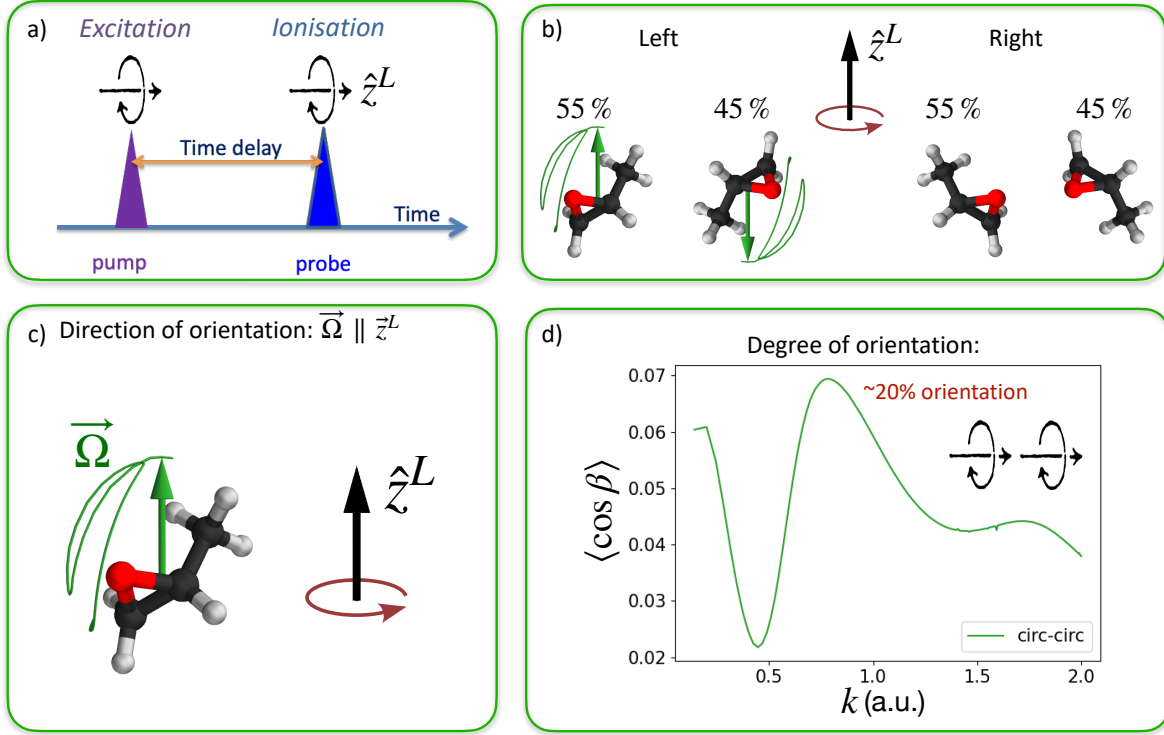


**Figure 4** Enantio-sensitive molecular orientation by excitation probed via photoionization. (a) Circularly polarized pulse ( $\hat{z}^L$  is the direction of photon spin in the laboratory frame) excites a superposition of LUMO and LUMO<sub>+1</sub> states in propylene oxide. (b) Circularly polarized probe removes the excited electron, leading to enantio-sensitive delay dependent orientation of cations. Molecules with  $\vec{\Omega} \parallel \hat{z}^L$  are excited and ionised preferentially. As a function of photoelectron energy, the tip of the curvature vector traces the green curve in space. This green curve illustrates the sequence of orientations achieved for different final photoelectron momenta from 0.25 to 2 a.u. Estimated percentages of "up" and "down" oriented species correspond to the maximal value of  $\langle \cos \beta \rangle \simeq 0.07$  and are obtained using the same model as in Ref. [16] (c) Direction of molecular orientation is defined by the curvature vector. (d) Expectation value  $\langle \cos \beta \rangle$  as a function of photoelectron momentum  $k$  (in atomic units). The values have been taken at the time-delay that maximizes  $\langle \hat{e}_{\Omega}^L \rangle$  and have been normalized to the total yield averaged over the pump-probe time delay.

where

$$\vec{\Omega}_{\text{exc}}^M(k, \rho) = -2C \text{Im} \left\{ \int d\Theta_k (\vec{D}_1 \cdot \vec{E}_{k1})^* (\vec{D}_2 \cdot \vec{E}_{k2}) e^{i\omega_{12}\tau} \right\} (\vec{d}_1^M \times \vec{d}_2^M), \quad (27)$$

$$\vec{\Omega}_{\text{ion}}^M(k, \rho) = -2C \text{Im} \left\{ (\vec{d}_1 \cdot \vec{E}_1)^* (\vec{d}_2 \cdot \vec{E}_2) e^{i\omega_{12}\tau} \int d\Theta_k \vec{D}_1^{*M} \times \vec{D}_2^M \right\}. \quad (28)$$

$$\begin{aligned} \vec{\Omega}_{\text{mix}}^M(k, \rho) = & -2C \text{Im} \left\{ \int d\Theta_k (\vec{d}_1 \cdot \vec{E}_1) (\vec{D}_2 \cdot \vec{E}_{k2})^* (\vec{D}_1^{*M} \times \vec{d}_2^M) e^{i\omega_{12}\tau} \right\} \\ & - 2C \text{Im} \left\{ \int d\Theta_k (\vec{D}_1 \cdot \vec{E}_{k1})^* (\vec{d}_2 \cdot \vec{E}_2) (\vec{d}_1^M \times \vec{D}_2^M) e^{i\omega_{12}\tau} \right\}, \end{aligned} \quad (29)$$

Here  $C \equiv |E_{\omega_{k_1}}||E_{\omega_1}||E_{\omega_{k_2}}||E_{\omega_2}|$ . Eq. (26) combines bound and continuum curvatures as detailed in Eqs. (14, 18), and also contains "mixed" terms, relying on both bound and continuum curvatures.

The orientationally averaged scalar product of the curvatures and a unit vector  $\vec{e}_\Omega$  are:

$$\langle \vec{\Omega}_{\text{exc}}(k, \rho) \cdot \vec{e}_\Omega \rangle = -\frac{1}{3} C \text{Re} \left\{ \int d\Theta_k \left( \vec{D}_1^* \cdot \vec{D}_2 \right) \right\} \left( \vec{d}_1 \times \vec{d}_2 \right) \cdot \vec{e}_\Omega \sin(\omega_{12}\tau), \quad (30)$$

$$\langle \vec{\Omega}_{\text{ion}}(k, \rho) \cdot \vec{e}_\Omega \rangle = -\frac{1}{3} C \left( \vec{d}_1 \cdot \vec{d}_2 \right) \vec{P}_{12}^+(k) \cdot \vec{e}_\Omega \sin(\omega_{12}\tau). \quad (31)$$

$$\begin{aligned} \langle \vec{\Omega}_{\text{mix}}(k, \rho) \cdot \vec{e}_\Omega \rangle = & -\frac{1}{3} C \text{Im} \left\{ \int d\Theta_k \left( \vec{d}_1 \cdot \vec{D}_2^* \right) \left( \vec{D}_1^* \times \vec{d}_2 \right) \cdot \vec{e}_\Omega e^{i\omega_{12}\tau} \right\} \\ & -\frac{1}{3} C \text{Im} \left\{ \int d\Theta_k \left( \vec{D}_1^* \cdot \vec{d}_2 \right) \left( \vec{d}_1 \times \vec{D}_2 \right) \cdot \vec{e}_\Omega e^{i\omega_{12}\tau} \right\}, \end{aligned} \quad (32)$$

One can verify that using the general expression for expectation value of  $\langle \vec{e}_\Omega^L \rangle^{\circ, \circ}$ :

$$\langle \vec{e}_\Omega^L \rangle^{\circ, \circ} = \sigma \left\langle \left( \vec{\Omega}^L \cdot \hat{z}^L \right) \vec{e}_\Omega^L \right\rangle \quad (33)$$

one obtains the same results as by evaluating  $\langle \vec{e}_\Omega^L \rangle^{\circ}$  explicitly without involving the curvature:

$$\begin{aligned} \langle \vec{e}_\Omega^L \rangle^{\circ} = & \frac{i\sigma}{30} C \int d\Theta_k \left\{ \left( \vec{d}_2 \cdot \vec{d}_1 \right) \left[ \vec{e}_\Omega \cdot \left( \vec{D}_2^* \times \vec{D}_1 \right) \right] + \left( \vec{D}_2^* \cdot \vec{D}_1 \right) \left[ \vec{e}_\Omega \cdot \left( \vec{d}_2 \times \vec{d}_1 \right) \right] \right. \\ & \left. + \left( \vec{d}_2 \cdot \vec{D}_1 \right) \left[ \vec{e}_\Omega \cdot \left( \vec{D}_2^* \times \vec{d}_1 \right) \right] + \left( \vec{D}_2^* \cdot \vec{d}_1 \right) \left[ \vec{e}_\Omega \cdot \left( \vec{d}_2 \times \vec{D}_1 \right) \right] \right\} e^{i\omega_{21}t} \hat{z} + \text{c.c.} \end{aligned} \quad (34)$$

Comparing this result to  $\langle \vec{\Omega}_{\text{mix}} \cdot \vec{e}_\Omega \rangle$  we find that the factor  $R^{(2, \circ, \circ)} = \frac{1}{10}$  is purely numerical due to preserved cylindrical symmetry:

$$\langle \vec{e}_\Omega^L \rangle^{\circ, \circ} = \sigma \left\langle \left( \vec{\Omega}^L \cdot \hat{z}^L \right) \vec{e}_\Omega^L \right\rangle = \sigma R^{(2, \circ, \circ)} \langle \vec{\Omega} \cdot \vec{e}_\Omega \rangle \hat{z}^L. \quad (35)$$

Finally, one can verify that the expression for the enantio-sensitive and dichroic yield  $W_{\circ, \circ}^{ES} - W_{\circ, \circ}^{ES}$  via geometric phase also remains invariant, because the sum of the curvatures (and the sum of the geometric phases) only contains terms independent of  $\sigma$ , just like the curvature and the geometric phase in the one-photon case:

$$W_{\circ, \circ}^{ES} - W_{\circ, \circ}^{ES} = \frac{\sigma}{4\pi} \int \left( \vec{\Omega}_{\circ, \circ}^M(k, \theta, \phi) + \vec{\Omega}_{\circ, \circ}^M(k, \theta, \phi) \right) \cdot d\vec{S}^M = \frac{\sigma}{4\pi} \left( \Phi_{\circ, \circ}^{ES} + \Phi_{\circ, \circ}^{ES} \right). \quad (36)$$

## 6. Opportunities for control of geometric observables

PI-MOCD is the first geometric observable that is directly proportional to the curvature, relying on the geometry of either bound or continuum states. Importantly, the curvature is a dynamical property, as it relies on the excitation of currents and reflects their temporal geometry. Dynamics offers several opportunities for the control. The direction of enantio-sensitive molecular orientation is defined by the direction of the curvature vector in the molecular frame. The curvature vectors relying on the vector product of bound or continuum dipoles naturally have different directions:  $\vec{\Omega}_{\text{exc}} \parallel \vec{d}_1 \times \vec{d}_2$  and  $\vec{\Omega}_{\text{ion}} \parallel \text{Re}\{\int d\Theta_k \vec{D}_1^* \times \vec{D}_2\}$ . Moreover, both orientations are state-specific (see Figs. 2,3 (b) for propylene oxide). It presents several opportunities for controlling the enantio-sensitive direction of molecular orientation.

First, by changing the frequency of the pump pulse, one can address different bound states and thus control both the magnitude and direction of the curvature. Second, controlling the polarization of the pump-probe pulse sequence also allows us to control the magnitude and the direction of the enantio-sensitive molecular orientation by switching the curvature between its form defined by the geometry of the excited bound states to the one defined by the geometry of the continuum states. Figs. 2 and 3 illustrate how the direction of the curvature and respective molecular orientation changes if one switches polarizations of pump and probe pulses from circular (linear) to linear (circular). Third, by changing the frequency of the probe pulse in case of linear-circular pulse sequence one can change the direction of the curvature as shown in Fig. 2(b).

For a given set of intermediate bound states excited by a pump pulse and continuum states populated by the probe pulse, the magnitudes of  $\vec{\Omega}_{\text{ion}}$  and  $\vec{\Omega}_{\text{exc}}$  differ only in their dipole factors. The bound transition dipole contributions to the magnitudes of  $\vec{\Omega}_{\text{ion}}$  and  $\vec{\Omega}_{\text{exc}}$  are  $\vec{d}_1 \cdot \vec{d}_2 = -7.3 \times 10^{-2}$  a.u. and  $|\vec{d}_1 \times \vec{d}_2| = 4.9 \times 10^{-2}$  a.u., respectively. The continuum dipole contributions  $\text{Re}\{\int d\Theta_k \vec{D}_1^* \cdot \vec{D}_2\}$  and  $|\text{Re}\{\int d\Theta_k \vec{D}_1^* \times \vec{D}_2\}|$  change as a function of the photoelectron energy and are shown in Fig. 5. These two parameters determine the  $k$ -dependence of expectation value of the degree of orientation in Figs. 2,3(c).

### Outlook

Geometric magnetism in chiral molecules appears to be a ubiquitous phenomenon, which can be controlled by tailoring light pulses and by addressing various molecular states. The linear-circular and circular-linear pump-probe sequences have been used experimentally to observe time-resolved photoelectron circular dichroism (TR-PECD) and photoexcitation circular dichroism (PXCD) in chiral molecules via detection of angular distribution of photoelectrons. We show that in both cases, the de-

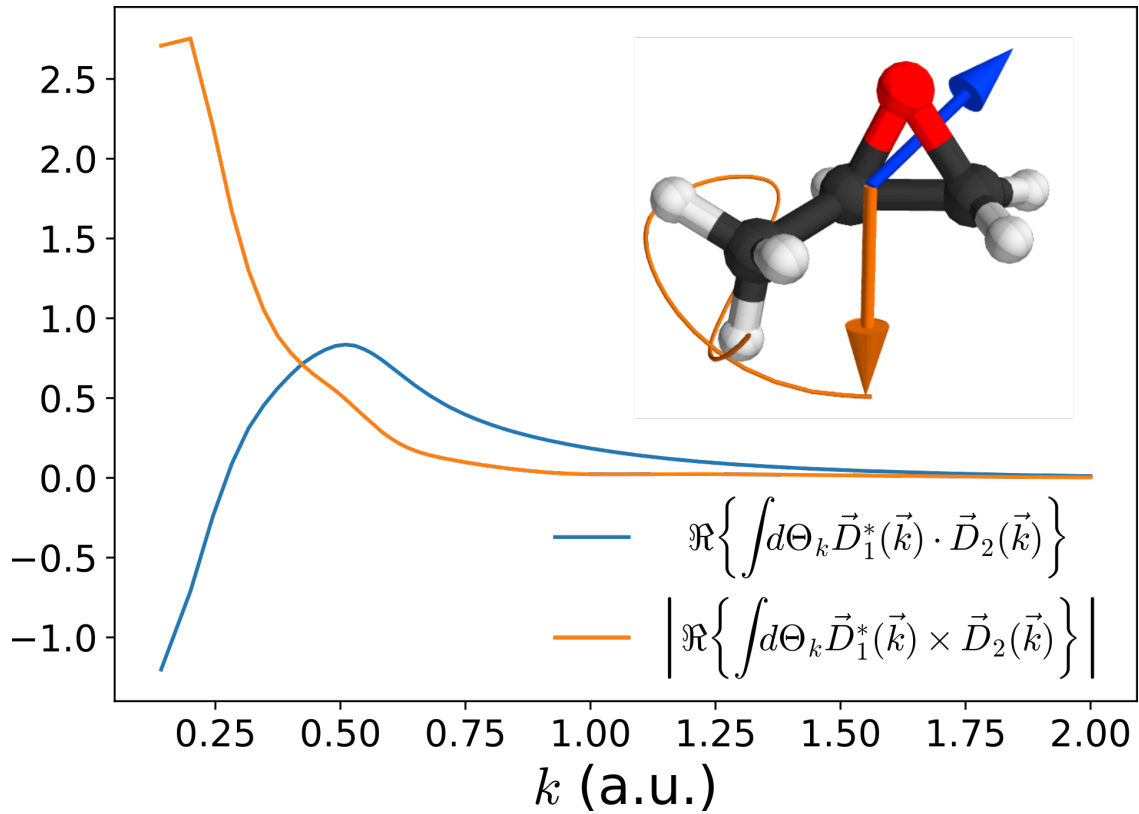


**Figure 5** Photoelectron momentum dependent terms  $\Re\{\int d\Theta_k \vec{D}_1^*(\vec{k}) \cdot \vec{D}_2(\vec{k})\}$  and  $|\Re\{\int d\Theta_k \vec{D}_1^*(\vec{k}) \times \vec{D}_2(\vec{k})\}|$ , controlling the PI-MOCD in case of circular-linear pulse sequence (blue) and linear-circular pulse sequence (orange). The inset shows the molecule together with the molecular axis getting oriented in each case;  $\vec{d}_1 \times \vec{d}_2$  in the circular-linear case (blue arrow), and  $\Re\{\int d\Theta_k \vec{D}_1^* \times \vec{D}_2\}$  in the linear-circular case (orange arrow). The latter changes as a function of photoelectron momentum  $k$  and is shown for  $k=0.2$  a.u. As  $k$  increases, the tip of the orange arrow traces the orange curve.

tection of molecular fragments leads to a complementary geometric observable, directly proportional to the curvature in continuum or bound states.

Our results show that the temporal evolution of angular distribution of fragments (Eqs. (21,22)) and angular distribution of photoelectrons produced after inducing the photo-excitation circular dichroism (circular-linear pump-probe sequence)[32] and controlled by the term  $\int d\Theta_k \vec{k} (\vec{D}_1^* \cdot \vec{D}_2)$  have fundamentally different properties.

The former is proportional to the current in the bound states  $\propto \sin(\omega_{12}\tau)$  and thus vanishes at zero pump-probe delay  $\tau = 0$ , while the latter also includes terms  $\propto \cos(\omega_{12}\tau)$  and does not vanish at  $\tau = 0$ . This property establishes PI-MOCD as a direct probe of charge-directed reactivity: PI-MOCD is proportional to the curvature (either in bound or in continuum states) and as such relies on time-reversal symmetry breaking, which can be introduced by exciting current prior to photoionization. The direction of current at the moment of ionization defines the orientation of molecular cations and

therefore the direction of molecular fragmentation, highlighting the ability of the ultrafast electron dynamics to control subsequent dynamics of the nuclei. Simulations [33] show that enantio-sensitive fragment asymmetry resulting from excitation of electronic wave-packet in Rydberg states in methyl lactate molecule in linear-circular polarization sequence reaches 20%, confirming strong enantio-sensitivity of curvature-driven geometric observables.

The control over the directions of enantio-sensitive orientations of molecular ions suggests new opportunities. For example, in linear-circular sequence of the pulses the tip of the curvature vector traces the orange curve in space (Fig. 3(b)) as a function of photoelectron energy. This orange curve illustrates the sequence of orientations of the curvature vector achieved for different final photoelectron momenta from 0.25 to 2 a.u. Since enantio-sensitive molecular orientation follows the orientation of the curvature vector, polarization controlled pulses at free electron lasers (FELs), such as chirped circularly polarized pulses, can be used to force molecular ions to draw the trajectory shown in Fig. 3(b) (see orange trajectory) within a single experiment. Alternately, the set of experiments in which the frequency of the probe circularly polarized light is tuned within several tens of eV will produce a variety of well controlled molecular orientations.

The geometric magnetism in bound states suggests new recipes for merging topological and enantio-sensitive response in chiral molecules. In particular, the flux of mixed curvature in the configurations space of laser field orientations emerging in the excitation by circularly polarized pump and probe pulses is proportional to the enantio-sensitive and dichroic part of the photoionization yield (Eqs. 10, 36). In analogy to the so-called Thouless charge pump, one would expect to realize a quantized rate of enantio-sensitive charge transfer via diabolic points in rotational states.

## Acknowledgments

We gratefully acknowledge many enlightening discussions with Prof. Misha Ivanov. We gratefully acknowledge Prof. Vladimir Chernyak for discussions and lectures on the topic. A.F.O. and D.A. acknowledge funding from the Royal Society (URF/R1/201333). O.S., A.R. P.M.M. gratefully acknowledge ERC-2021-AdG project ULISSES, grant agreement No 101054696.

## Appendices

### Appendix A: Closed lift for a state vector $|\psi_{el}(t)\rangle \langle \psi_{el}(t)|$

The closed lift is a concept from fiber bundle theory that allows one to identify the geometric phase outside the approximation of an adiabatic evolution.

In the Aharonov-Anandan fiber bundle theory, one introduces the base space in which all pure state vectors  $|\psi_{el}(t)\rangle \langle \psi_{el}(t)|$  live. By definition, the state vectors do not possess any phase. Thus, when the system evolves along the closed contour in the base space, the state vector remains the same after this cyclic evolution along the contour  $\gamma$ :  $|\psi_{el}(t)\rangle \langle \psi_{el}(t)| = |\psi_{el}(t+T)\rangle \langle \psi_{el}(t+T)|$ .

Wave-functions corresponding to state vectors  $|\psi_{el}(t)\rangle \langle \psi_{el}(t)|$  at every point in base space  $|\psi_{el}(t)\rangle e^{i\phi}$  "live" on a fiber, which "grows vertically" from the base space while the phase  $\phi$  is taking all possible values along this vertical direction (the fiber). These wave-functions are said to constitute "lifts" of the state vector  $|\psi_{el}(t)\rangle \langle \psi_{el}(t)|$  from the base space into the fiber space (at every point on the contour  $\gamma$  in the base space). The wave-function that does not accumulate a phase as a result of cyclic evolution of a state vector on the contour  $\gamma$  such that  $|\psi_{el}^0(t)\rangle = |\psi_{el}^0(t+T)\rangle$  is called a closed lift.

We can show that the wave-function  $\psi_{el}^0(t, \vec{E}(\rho), \vec{r})$  defined by Eq. (46) does not accumulate a phase as a result of cyclic evolution of rotational degrees of freedom and therefore presents the closed lift of the state vector  $|\psi_{el}(t)\rangle \langle \psi_{el}(t)|$ .

In our case, one cycle of evolution corresponds to one full rotation of the molecular frame  $\psi_{el}^0(t, \vec{E}(\rho), \vec{r})$  from some initial orientation characterised by Euler angles  $\rho_0 = \{\theta_0, \phi_0, \alpha_0\}$  with respect to the lab frame to the exact same orientation  $\rho_0 + 2\pi = \{\theta_0, \alpha_0 + 2\pi, \phi_0 + 2\pi\}$ . The wave-functions  $\psi_{el}^0(t, \vec{E}(\rho_0), \vec{r})$  and  $\psi_{el}^0(t, \vec{E}(\rho_0 + 2\pi), \vec{r})$  can be obtained from the same lab-frame wave-function using an appropriate sequence of unitary transformations, such as e.g. rotation around  $\hat{n}$ -axes by the angle  $\xi$ :  $\psi_{el}^0(t, \vec{E}(\rho_0 + 2\pi), \vec{r}) = e^{-i\xi(\hat{n}\cdot\hat{L})}\psi_{el}^0(t, \vec{r}) = \psi_{el}^0(t, \vec{E}(\rho_0), \vec{r})$ . Since these unitary transformations do not impart any relative phases on the transformed wave-functions  $\psi_{el}^0(t, \vec{E}(\rho_0 + 2\pi), \vec{r})$  and  $\psi_{el}^0(t, \vec{E}(\rho_0), \vec{r})$ , and the same arguments remain valid for every point  $\rho_0$ , the wave-function  $\psi_{el}^0(t, \vec{E}(\rho), \vec{r})$  presents a closed lift.

## Appendix B: Derivation of Eq. (6)

Previously, we have derived Eqs. (5, 7) using the concept of adiabatic evolution of the rotational degree of freedom, introducing two different time scales for the evolution of electronic and rotational degrees of freedom. We now extend our derivation to a general case, including non-adiabatic evolution. We follow the arguments of Ref. [31] and introduce a rotational Hamiltonian  $H_{rot}(t)$ , responsible for the cyclic non-adiabatic evolution of the rotational wave-function  $\psi_{rot}(\rho, t)$ :

$$i\frac{d}{dt}\psi_{rot}(\rho, t) = H_{rot}(t)\psi_{rot}(\rho, t). \quad (37)$$

For example,  $H_{rot}(t)$  could encapsulate a sequence of microwave fields driving resonant transitions in three rotational levels of a chiral molecule. Since our focus is laser-induced coupling between electronic and rotational degrees of freedom, which arises due to the sensitivity of the electronic dynamics to the mutual orientation between the molecule and the laser field, we omit the standard Coriolis coupling between electronic and rotational degrees of freedom in the zero approximation. Starting from the TDSE for the full wave-function including the electronic and rotational degrees of freedom:

$$i\frac{d}{dt}\Psi(\vec{r},\rho,t) = \left[ H_{el} + \vec{r} \cdot \vec{E}(\rho,t) + H_{rot}(t) \right] \Psi(\vec{r},\rho,t) \quad (38)$$

and using the ansatz:

$$\Psi(\vec{r},\rho,t) = \psi_{el}(\vec{r},\rho,t) \psi_{rot}(\rho,t), \quad (39)$$

we first obtain

$$i\psi_{rot}(\rho,t)\frac{d}{dt}\psi_{el}(\vec{r},\rho,t) + i\psi_{el}(\vec{r},\rho,t)\frac{d}{dt}\psi_{rot}(\rho,t) = \left[ H_{el} + \vec{r} \cdot \vec{E}(\rho,t) + H_{rot}(t) \right] \psi_{el}(\vec{r},\rho,t) \psi_{rot}(\rho,t). \quad (40)$$

Multiplying the TDSE (Eq. (40)) by  $\psi_{rot}^*(\rho,t)$  from the left and integrating over  $\rho$  yields the following equation:

$$\begin{aligned} i \int d\rho |\psi_{rot}(\rho,t)|^2 \frac{d}{dt} \psi_{el}(\vec{r},\rho,t) + i \int d\rho \psi_{el}(\vec{r},\rho,t) \psi_{rot}^*(\rho,t) \frac{d}{dt} \psi_{rot}(\rho,t) = & \quad (41) \\ \int d\rho \psi_{rot}^*(\rho,t) \left[ H_{el} + \vec{r} \cdot \vec{E}(\rho,t) \right] \psi_{el}(\vec{r},\rho,t) \psi_{rot}(\rho,t) & \\ - i \int d\rho \frac{d}{dt} [\psi_{rot}^*(\rho,t)] \psi_{el}(\vec{r},\rho,t) \psi_{rot}(\rho,t), & \end{aligned}$$

where we have used Eq. (37) in the last term applying the rotational Hamiltonian  $H_{rot}(t)$  to the bra-vector on the left. Note, that in doing so we have avoided the assumption of the adiabatic decoupling of the electronic and rotational degrees of freedom. Indeed, the adiabatic decoupling implies that  $H_{rot}$  does not affect the electronic wave-function, while here it clearly does so via the last term in Eq. (41). In the following we shall use the adiabatic decoupling to derive the equation for the closed lift solution (see Eqs. (45-47)).

Eq. (41) takes the following form:

$$\begin{aligned} i \int d\rho |\psi_{rot}(\rho,t)|^2 \frac{d}{dt} \psi_{el}(\vec{r},\rho,t) + i \int d\rho \psi_{el}(\vec{r},\rho,t) \frac{d}{dt} |\psi_{rot}(\rho,t)|^2 = & \quad (42) \\ \int d\rho \psi_{rot}^*(\rho,t) \left[ H_{el} + \vec{r} \cdot \vec{E}(\rho,t) \right] \psi_{el}(\vec{r},\rho,t) \psi_{rot}(\rho,t). & \end{aligned}$$

We shall now assume that the rotational wave-packet is narrow. This assumption can be realized in an experiment by preparing a narrow rotational wavepacket with a pump pulse and using a short probe pulse with time-dependent polarization, rotating with respect to the frame established by the pump pulse. Introducing  $\dot{\bar{\rho}}(t) \equiv \int d\rho \frac{d}{dt} |\psi_{rot}(\rho, t)|^2 \rho = \frac{d}{dt} \int d\rho |\psi_{rot}(\rho, t)|^2 \rho = \frac{d}{dt} \bar{\rho}(t)$  and expanding  $E_i(\rho, t) = E_i(\rho_0, t) + \nabla_{\rho_0} E_i(\rho_0, t)(\rho - \rho_0)$ , and  $\psi_{el}(\vec{r}, \rho, t)$  up to the first order around  $\bar{\rho}(t)$ , we obtain for the integral  $\int d\rho \psi_{el}(\vec{r}, \rho, t) \frac{d}{dt} |\psi_{rot}(\rho, t)|^2$  the following expansion:

$$\int d\rho \psi_{el}(\vec{r}, \rho, t) \frac{d}{dt} |\psi_{rot}(\rho, t)|^2 = \int d\rho \psi_{el}(\vec{r}, \bar{\rho}(t), t) \frac{d}{dt} |\psi_{rot}(\rho, t)|^2 + \nabla_{\bar{\rho}} \psi_{el}(\vec{r}, \bar{\rho}(t), t) \cdot \dot{\bar{\rho}}(t). \quad (43)$$

Here we took into account that  $\int d\rho |\psi_{rot}(\rho, t)|^2 = 1$ , which leads to  $\frac{d}{dt} \int d\rho |\psi_{rot}(\rho, t)|^2 = 0$ . Combining this term with the other terms, we obtain the following TDSE for the "global" wave-function  $\psi_{el}(\vec{r}, \bar{\rho}(t), t)$ :

$$i \frac{\partial}{\partial t} \psi_{el}(\vec{r}, \bar{\rho}(t), t) + i \nabla_{\bar{\rho}} \psi_{el}(\vec{r}, \bar{\rho}(t), t) \cdot \dot{\bar{\rho}}(t) = \left[ H_{el} + \vec{r} \cdot \vec{E}(\bar{\rho}(t), t) \right] \psi_{el}(\vec{r}, \bar{\rho}(t), t). \quad (44)$$

Note that  $\bar{\rho}(t) = \int d\rho \rho |\psi_{rot}(\rho, t)|^2$  follows the evolution of the center of the rotational wave-packet and therefore is controlled by  $H_{rot}(t)$ .

Let's derive an approximate solution  $\psi_{el}^0(\vec{r}, \rho, t)$  for the case when the rotational Hamiltonian itself does not affect the electronic dynamics, i.e.

$$H_{rot}(t) \psi_{el}^0(\vec{r}, \rho, t) \psi_{rot}(\rho, t) = \psi_{el}^0(\vec{r}, \rho, t) H_{rot}(t) \psi_{rot}(\rho, t). \quad (45)$$

Applying this condition to Eq. (40) yields

$$i \psi_{rot}(\rho, t) \frac{d}{dt} \psi_{el}^0(\vec{r}, \rho, t) = \left[ H_{el} + \vec{r} \cdot \vec{E}(\rho, t) \right] \psi_{el}^0(\vec{r}, \rho, t) \psi_{rot}(\rho, t), \quad (46)$$

demonstrating that  $\psi_{el}^0(\vec{r}, \rho, t)$  solves the "local" TDSE for fixed  $\rho$ :

$$i \frac{d}{dt} \psi_{el}^0(\vec{r}, \rho, t) = \left[ H_{el} + \vec{r} \cdot \vec{E}(\rho, t) \right] \psi_{el}^0(\vec{r}, \rho, t). \quad (47)$$

Comparing Eq. (44) with Eq. (46) we find that the "global" and the "local" solutions are related as follows:

$$\psi_{el}(\vec{r}, \bar{\rho}(t), t) = e^{iS(\bar{\rho}(t))} \psi_{el}^0(\vec{r}, \bar{\rho}(t), t). \quad (48)$$

Substituting Eq. (48) to Eq. (44), we find:

$$S(\bar{\rho}(t)) = i \int_{\bar{\rho}(t_0)}^{\bar{\rho}(t)} d\rho' \langle \psi_{el}^0(\vec{r}, \rho', t) | \nabla_{\rho'} \psi_{el}^0(\vec{r}, \rho', t) \rangle, \quad (49)$$

Note that, by the virtue of equations Eq. (45) and Eq. (46), the only reason why  $\psi_{el}^0(\vec{r}, \rho, t)$  depends on  $\rho$  is because the laser field in the molecular frame depends on  $\rho$ , i.e.  $\psi_{el}^0(\vec{r}, \rho, t) \equiv \psi_{el}^0(\vec{r}, \vec{E}(\rho), t)$ .

Indeed,  $\psi_{el}^0(\vec{r}, \rho, t)$  satisfies the TDSE for the electronic degrees of freedom Eq.47. This equation, by definition, has no information about the rotational degree of freedom. Thus, the gradient of  $\psi_{el}^0(\vec{r}, \rho, t)$  with respect to  $\rho$  can be rewritten in an equivalent form,  $\nabla_{\rho} \psi_{el}^0(\vec{r}, \rho, t) = \nabla_{\vec{E}} \psi_{el}^0(\vec{r}, \rho, t) \frac{\partial \vec{E}}{\partial \rho}$ , as long as the laser field  $\vec{E}$  can be used to unambiguously define the laboratory frame with respect to which the molecular orientation  $\rho$  is expressed. For example, circularly (elliptically) polarized field  $\vec{E}$  satisfies this requirement. Hence the derivative should be taken with respect to  $\vec{E}$ . This leads to the following equivalent expression for the geometric phase:

$$S(\bar{\rho}(t)) = i \int_{\vec{E}(t_0)}^{\vec{E}(t)} \langle \psi_{el}^0(\vec{r}, \rho', t) | \nabla_{\vec{E}} \psi_{el}^0(\vec{r}, \rho', t) \rangle d\vec{E} \equiv \int_{\vec{E}(t_0)}^{\vec{E}(t)} \vec{A}(\vec{E}) \cdot d\vec{E}, \quad (50)$$

where  $\vec{A}(\vec{E}) = \langle \psi_{el}^0(\vec{r}, \vec{E}, t) | \nabla_{\vec{E}} \psi_{el}^0(\vec{r}, \vec{E}, t) \rangle$ .

### Appendix C: Time-reversal symmetry

To prove Eq. (20) we extend the approach established in [16] and introduce an operator  $\hat{G}$ :

$$\int d\Theta_k \vec{D}_1^*(\vec{k}) \cdot \vec{D}_2(\vec{k}) = \int d\Theta_k \langle \psi_k | \vec{r} | \psi_1 \rangle^* \cdot \langle \psi_k | \vec{r} | \psi_2 \rangle \quad (51)$$

$$= \int d\Theta_k \langle \psi_1 | \vec{r} | \psi_k \rangle \cdot \langle \psi_k | \vec{r} | \psi_2 \rangle \quad (52)$$

$$= \int d\Theta_k \langle \psi_1 | r_i P_k r_i | \psi_2 \rangle \quad (53)$$

$$= \langle \psi_1 | r_i P_k r_i | \psi_2 \rangle \quad (54)$$

$$= \langle \psi_1 | \hat{G} | \psi_2 \rangle \quad (55)$$

We can now test the properties of this operator with respect to time-reversal symmetry.

$$\hat{G} \equiv \hat{r}_i \hat{P}_k \hat{r}_i \quad (56)$$

$$\hat{G}^\dagger = \hat{r}_i^\dagger \hat{P}_k^\dagger \hat{r}_i^\dagger = \hat{r}_i \hat{P}_k \hat{r}_i = \hat{G} \quad (57)$$

$$[\hat{P}_k, \hat{T}] = [\hat{r}_i, \hat{T}] = 0 \Rightarrow [\hat{G}, \hat{T}] = 0 \quad (58)$$

$$\langle \alpha | \hat{G} | \beta \rangle = \langle \tilde{\alpha} | \hat{G} | \tilde{\beta} \rangle^* \quad (59)$$

For  $|\alpha\rangle = |\tilde{\alpha}\rangle$  and  $|\beta\rangle = |\tilde{\beta}\rangle$ , we get  $\langle \alpha | \hat{G} | \beta \rangle = \langle \alpha | \hat{G} | \beta \rangle^*$ , thus  $\langle \alpha | \hat{G} | \beta \rangle \in \mathbb{R}$ . This results yields Eq. (20).

#### Appendix D: Orientational averaging, derivation of Eq. (16) and Eq. (15)

We shall use the following expressions:

$$\int d\rho l_{i\alpha} l_{j\beta} l_{k\gamma} l_{l\delta} = \frac{1}{30} \begin{pmatrix} \delta_{ij}\delta_{kl} & \delta_{ik}\delta_{jl} & \delta_{il}\delta_{jk} \end{pmatrix} \begin{pmatrix} 4 & -1 & -1 \\ -1 & 4 & -1 \\ -1 & -1 & 4 \end{pmatrix} \begin{pmatrix} \delta_{\alpha\beta}\delta_{\gamma\delta} \\ \delta_{\alpha\gamma}\delta_{\beta\delta} \\ \delta_{\alpha\delta}\delta_{\beta\gamma} \end{pmatrix} \quad (60)$$

$$= \frac{1}{30} \left[ 4\delta_{ij}\delta_{kl}\delta_{\alpha\beta}\delta_{\gamma\delta} - \delta_{ik}\delta_{jl}\delta_{\alpha\beta}\delta_{\gamma\delta} - \delta_{il}\delta_{jk}\delta_{\alpha\beta}\delta_{\gamma\delta} \right. \quad (61)$$

$$\left. - \delta_{ij}\delta_{kl}\delta_{\alpha\gamma}\delta_{\beta\delta} + 4\delta_{ik}\delta_{jl}\delta_{\alpha\gamma}\delta_{\beta\delta} - \delta_{il}\delta_{jk}\delta_{\alpha\gamma}\delta_{\beta\delta} \right. \quad (62)$$

$$\left. - \delta_{ij}\delta_{kl}\delta_{\alpha\delta}\delta_{\beta\gamma} - \delta_{ik}\delta_{jl}\delta_{\alpha\delta}\delta_{\beta\gamma} + 4\delta_{il}\delta_{jk}\delta_{\alpha\delta}\delta_{\beta\gamma} \right], \quad (63)$$

i.e.,

$$\begin{aligned} & \int d\rho (\vec{a}^L \cdot \vec{u}^L)(\vec{b}^L \cdot \vec{v}^L)(\vec{w}^L \cdot \vec{c}^L) \vec{x}^L \\ &= \frac{1}{30} \left[ 4(\vec{a}^L \cdot \vec{b}^L) \vec{c}^L (\vec{u}^M \cdot \vec{v}^M) (\vec{w}^M \cdot \vec{x}^M) \right. \\ & \quad - (\vec{a}^L \cdot \vec{c}^L) \vec{b}^L (\vec{u}^M \cdot \vec{v}^M) (\vec{w}^M \cdot \vec{x}^M) \\ & \quad - (\vec{b}^L \cdot \vec{c}^L) \vec{a}^L (\vec{u}^M \cdot \vec{v}^M) (\vec{w}^M \cdot \vec{x}^M) \\ & \quad - (\vec{a}^L \cdot \vec{b}^L) \vec{c}^L (\vec{u}^M \cdot \vec{w}^M) (\vec{v}^M \cdot \vec{x}^M) \\ & \quad + 4(\vec{a}^L \cdot \vec{c}^L) \vec{b}^L (\vec{u}^M \cdot \vec{w}^M) (\vec{v}^M \cdot \vec{x}^M) \\ & \quad - (\vec{b}^L \cdot \vec{c}^L) \vec{a}^L (\vec{u}^M \cdot \vec{w}^M) (\vec{v}^M \cdot \vec{x}^M) \\ & \quad - (\vec{a}^L \cdot \vec{b}^L) \vec{c}^L (\vec{u}^M \cdot \vec{x}^M) (\vec{v}^M \cdot \vec{w}^M) \\ & \quad - (\vec{a}^L \cdot \vec{c}^L) \vec{b}^L (\vec{u}^M \cdot \vec{x}^M) (\vec{v}^M \cdot \vec{w}^M) \\ & \quad \left. + 4(\vec{b}^L \cdot \vec{c}^L) \vec{a}^L (\vec{u}^M \cdot \vec{x}^M) (\vec{v}^M \cdot \vec{w}^M) \right]. \end{aligned} \quad (64)$$

We derive Eq. (16), which we list here for completeness:

$$\langle \vec{e}_\Omega^L \rangle^{\uparrow, \circ} = \sigma \left\langle \left( \vec{\Omega}_{\text{ion}} \cdot \hat{z}^L \right) \vec{e}_\Omega^L \right\rangle = \sigma \text{Rv} \langle \vec{\Omega}_{\text{ion}} \cdot \vec{e}_\Omega \rangle \hat{z}^L, \quad (65)$$

where

$$\vec{\Omega}_{\text{ion}}(k, \rho) = -|E_{\omega_{k_1}}| |E_{\omega_{k_2}}| \left( \vec{d}_1 \cdot \vec{e}_1 \right)^* \left( \vec{d}_2 \cdot \vec{e}_2 \right) \vec{P}_{12}^+(k) \sin(\omega_{12} \tau), \quad (66)$$

(Eq. (14)). Substituting Eq. (66) into Eq. (65) we obtain:

$$\langle \vec{e}_\Omega^L \rangle^{\uparrow, \circ} = -|E_{\omega_{k_1}}| |E_{\omega_{k_2}}| \sin(\omega_{12} \tau) \int d\rho \left( \vec{d}_1^L \cdot \vec{e}_1^L \right)^* \left( \vec{d}_2^L \cdot \vec{e}_2^L \right) \left( \vec{P}_{12}^{+L}(k) \cdot \hat{z}^L \right) \vec{e}_\Omega^L \quad (67)$$

Applying Eq. (64) to Eq. (67) we obtain

$$\langle \vec{e}_\Omega \rangle^{\uparrow, \circ} = \frac{\sigma}{30} C \left[ 4 \left( \vec{d}_2 \cdot \vec{d}_1 \right) \vec{e}_\Omega^M - \left( \vec{d}_2 \cdot \vec{e}_\Omega^M \right) \vec{d}_1 - \left( \vec{d}_1 \cdot \vec{e}_\Omega^M \right) \vec{d}_2 \right] \cdot \vec{P}_{12}^+(k) \sin(\omega_{12} \tau) \hat{z}^L, \quad (68)$$

which is up to notations  $\vec{P}_{12}^+(k) = v |\vec{P}_{12}^+(k)| \vec{e}_\Omega$  is equivalent to Eq. (16).

Starting from

$$\vec{\Omega}_{\text{ion}}(k, \rho) \cdot \vec{e}_\Omega^M = -|E_{\omega_{k_1}}| |E_{\omega_{k_2}}| \left( \vec{d}_1 \cdot \vec{e}_1 \right)^* \left( \vec{d}_2 \cdot \vec{e}_2 \right) \left( \vec{P}_{12}^+(k) \cdot \vec{e}_\Omega^M \right) \sin(\omega_{12} \tau), \quad (69)$$

we shall now evaluate  $\langle \vec{\Omega}_{\text{ion}} \cdot \vec{e}_\Omega^M \rangle$ . Note that we only need to average the part that depends on mutual orientations of the pump pulse and molecule:

$$\int d\rho \left( \vec{d}_1 \cdot \vec{e}_1 \right)^* \left( \vec{d}_2 \cdot \vec{e}_2 \right) = \frac{1}{3} \left( \vec{d}_1 \cdot \vec{d}_2 \right) \left( \vec{e}_1^* \cdot \vec{e}_2 \right) = \frac{1}{3} \left( \vec{d}_1 \cdot \vec{d}_2 \right) |\mathcal{E}_{\omega_1}| |\mathcal{E}_{\omega_2}|, \quad (70)$$

yielding Eq. (15):

$$\langle \vec{\Omega}_{\text{ion}}(k) \cdot \vec{e}_\Omega \rangle = -\frac{1}{3} \sigma v C \left( \vec{d}_1 \cdot \vec{d}_2 \right) |\vec{P}_{12}^+(k)| \sin(\omega_{12} \tau). \quad (71)$$

## Appendix E: Connection between the curvature and the photoionization yield

In this section, we calculate the photoionization yield  $W \equiv \int |a_{\vec{k}}|^2 d\Theta_k$  for two-photon processes considered in this work. For example, consider a sequence of linear and circularly polarized pulses:

$$\vec{\mathcal{E}}_i^L = \mathcal{E}_{\omega_i} \hat{x}^L, \quad \vec{E}_j^L = E_{\omega_{jk}} \frac{1}{\sqrt{2}} (\hat{x}^L + i\sigma \hat{y}^L) \quad (72)$$

The photoionization amplitude  $|a_{\vec{k}}|^2$  can be written as:

$$\begin{aligned} |a_{\vec{k}}|^2 &= \frac{1}{2} [|E_{\omega_{1k}}|^2 |(\vec{d}_1^L \cdot \vec{\mathcal{E}}_1^L)|^2 \left[ |\vec{D}_1^L \cdot \hat{x}^L|^2 + |\vec{D}_1^L \cdot \hat{y}^L|^2 + i\sigma (\vec{D}_1^{*L} \times \vec{D}_1^L) \cdot \hat{z}^L \right] \\ &\quad + \frac{1}{2} [|E_{\omega_{2k}}|^2 |(\vec{d}_2^L \cdot \vec{\mathcal{E}}_2^L)|^2 \left[ |\vec{D}_2^L \cdot \hat{x}^L|^2 + |\vec{D}_2^L \cdot \hat{y}^L|^2 + i\sigma (\vec{D}_2^{*L} \times \vec{D}_2^L) \cdot \hat{z}^L \right] \\ &+ \text{Re} \left\{ E_{\omega_{1k}}^* E_{\omega_{2k}} (\vec{d}_1^L \cdot \vec{\mathcal{E}}_1^L)^* \cdot (\vec{d}_2^L \cdot \vec{\mathcal{E}}_2^L) \left[ (\vec{D}_1^{*L} \cdot \hat{x}^L) (\vec{D}_2^L \cdot \hat{x}^L) + (\vec{D}_1^{*L} \cdot \hat{y}^L) (\vec{D}_2^L \cdot \hat{y}^L) + i\sigma (\vec{D}_1^{*L} \times \vec{D}_2^L) \cdot \hat{z}^L \right] \right\} \end{aligned} \quad (73)$$

The dichroic (i.e. proportional to  $\sigma$ ) photoionization yield is

$$\int |a_{\vec{k}}|^2 d\Theta_k = \sigma \text{Re} \left\{ E_{\omega_{1k}}^* E_{\omega_{2k}} (\vec{d}_1^L \cdot \vec{\mathcal{E}}_1^L)^* \cdot (\vec{d}_2^L \cdot \vec{\mathcal{E}}_2^L) \left[ e^{i\omega_{12}\tau} \int i (\vec{D}_1^{*L} \times \vec{D}_2^L) d\Theta_k \right] \right\} \cdot \hat{z}^L = \sigma \vec{\Omega}^L \cdot \hat{z}^L, \quad (74)$$

where  $\vec{\Omega}$  is given by Eq. (14).

Next, consider a sequence of two circularly polarized pulses of the form

$$\vec{E}_j^L = E_{\omega_j} \frac{1}{\sqrt{2}} (\hat{x}^L + i\sigma \hat{y}^L), \quad \vec{E}_{\vec{k}j}^L = E_{\omega_{\vec{k}j}} \frac{1}{\sqrt{2}} (\hat{x}^L + i\sigma \hat{y}^L). \quad (75)$$

The photoionization amplitude  $|a_{\vec{k}}|^2$  can be written as:

$$|a_{\vec{k}}|^2 = |\vec{d}_1^L \cdot \vec{E}_1^L|^2 |\vec{D}_1^L \cdot \vec{E}_{\vec{k}1}^L|^2 + |\vec{d}_2^L \cdot \vec{E}_2^L|^2 |\vec{D}_2^L \cdot \vec{E}_{\vec{k}2}^L|^2 + 2 \text{Re} \left\{ (\vec{D}_1^L \cdot \vec{E}_{\vec{k}1}^L)^* (\vec{d}_1^L \cdot \vec{E}_1^L)^* (\vec{D}_2^L \cdot \vec{E}_{\vec{k}2}^L) (\vec{d}_2^L \cdot \vec{E}_2^L) \right\} \quad (76)$$

$$\begin{aligned} &= |\vec{d}_1^L \cdot \vec{E}_1^L|^2 |\vec{D}_1^L \cdot \vec{E}_{\vec{k}1}^L|^2 + |\vec{d}_2^L \cdot \vec{E}_2^L|^2 |\vec{D}_2^L \cdot \vec{E}_{\vec{k}2}^L|^2 + \frac{1}{2} \text{Re} \left\{ (\vec{D}_1^L \cdot \vec{E}_{\vec{k}1}^L)^* (\vec{d}_1^L \cdot \vec{E}_1^L)^* (\vec{D}_2^L \cdot \vec{E}_{\vec{k}2}^L) (\vec{d}_2^L \cdot \vec{E}_2^L) \right\} \\ &\quad + \frac{1}{2} \text{Re} \left\{ (\vec{d}_1^L \cdot \vec{E}_1^L)^* (\vec{D}_1^L \cdot \vec{E}_{\vec{k}1}^L)^* (\vec{d}_2^L \cdot \vec{E}_2^L) (\vec{D}_2^L \cdot \vec{E}_{\vec{k}2}^L) \right\} \end{aligned} \quad (77)$$

The part of the photoionization yield proportional to  $\sigma$  or  $\sigma^2$  is

$$\begin{aligned}
W_\sigma = \int d\Theta_k \frac{C}{2} \left\{ \right. & \left[ (\vec{d}_1^{*L} \cdot \hat{x}^L)(\vec{d}_2^L \cdot \hat{x}^L) + (\vec{d}_1^{*L} \cdot \hat{y}^L)(\vec{d}_2^L \cdot \hat{y}^L) \right] i\sigma (\vec{D}_1^* \times \vec{D}_2^L) \cdot \hat{z}^L e^{i\omega_{12}\tau} \\
& + \left[ (\vec{D}_1^* \cdot \hat{x}^L)(\vec{D}_2^L \cdot \hat{x}^L) + (\vec{D}_1^* \cdot \hat{y}^L)(\vec{D}_2^L \cdot \hat{y}^L) \right] i\sigma (\vec{d}_1^{*L} \times \vec{d}_2^L) \cdot \hat{z}^L e^{i\omega_{12}\tau} \\
& + \left[ (\vec{d}_2^{*L} \cdot \hat{x}^L)(\vec{D}_1^L \cdot \hat{x}^L) + (\vec{d}_2^{*L} \cdot \hat{y}^L)(\vec{D}_1^L \cdot \hat{y}^L) \right] i\sigma (\vec{D}_2^{*L} \times \vec{d}_1^L) \cdot \hat{z}^L e^{i\omega_{12}\tau} \\
& + \left[ (\vec{D}_2^{*L} \cdot \hat{x}^L)(\vec{d}_1^L \cdot \hat{x}^L) + (\vec{D}_2^{*L} \cdot \hat{y}^L)(\vec{d}_1^L \cdot \hat{y}^L) \right] i\sigma (\vec{d}_2^{*L} \times \vec{D}_1^L) \cdot \hat{z}^L e^{i\omega_{12}\tau} \\
& - \sigma^2 \left[ (\vec{d}_1^{*L} \times \vec{d}_2^L) \cdot \hat{z}^L \right] \left[ (\vec{D}_1^* \times \vec{D}_2^L) \cdot \hat{z}^L \right] e^{i\omega_{12}\tau} \\
& - \sigma^2 \left[ (\vec{D}_2^{*L} \times \vec{d}_1^L) \cdot \hat{z}^L \right] \left[ (\vec{d}_2^{*L} \times \vec{D}_1^L) \cdot \hat{z}^L \right] e^{i\omega_{12}\tau} \\
& \left. \right\} + \text{c.c.} \tag{78}
\end{aligned}$$

where  $C \equiv |E_{\omega_{k_1}}| |E_{\omega_1}| |E_{\omega_{k_2}}| |E_{\omega_2}|$ .

Let us prove Eq. (9) for circular pump and probe fields, using the yield (Eq. (78)) and the curvature (Eq. (26)). To this end, we calculate the expression

$$\begin{aligned}
\sigma \Omega^L(\rho) \cdot \hat{z}^L = \frac{C}{2} \int d\Theta_k \left\{ \right. & \left[ (\vec{d}_1^L \cdot \hat{x}^L)(\vec{d}_2^L \cdot \hat{x}^L) + (\vec{d}_1^L \cdot \hat{y}^L)(\vec{d}_2^L \cdot \hat{y}^L) \right] i\sigma (\vec{D}_1^{*L} \times \vec{D}_2^L) \cdot \hat{z}^L e^{i\omega_{12}\tau} \\
& + \left[ (\vec{D}_1^{*L} \cdot \hat{x}^L)(\vec{D}_2^L \cdot \hat{x}^L) + (\vec{D}_1^{*L} \cdot \hat{y}^L)(\vec{D}_2^L \cdot \hat{y}^L) \right] i\sigma (\vec{d}_1^L \times \vec{d}_2^L) \cdot \hat{z}^L e^{i\omega_{12}\tau} \\
& + \left[ (\vec{d}_1^L \cdot \hat{x}^L)(\vec{D}_2^L \cdot \hat{x}^L) + (\vec{d}_1^L \cdot \hat{y}^L)(\vec{D}_2^L \cdot \hat{y}^L) \right] i\sigma (\vec{D}_1^{*L} \times \vec{d}_2^L) \cdot \hat{z}^L e^{i\omega_{12}\tau} \\
& + \left[ (\vec{D}_1^{*L} \cdot \hat{x}^L)(\vec{d}_2^L \cdot \hat{x}^L) + (\vec{D}_1^{*L} \cdot \hat{y}^L)(\vec{d}_2^L \cdot \hat{y}^L) \right] i\sigma (\vec{d}_1^L \times \vec{D}_2^L) \cdot \hat{z}^L e^{i\omega_{12}\tau} \\
& - 2\sigma^2 (\vec{d}_1^L \times \vec{d}_2^L) \cdot \hat{z}^L (\vec{D}_1^{*L} \times \vec{D}_2^L) \cdot \hat{z}^L e^{i\omega_{12}\tau} \\
& - 2\sigma^2 (\vec{D}_1^{*L} \times \vec{d}_2^L) \cdot \hat{z}^L (\vec{d}_1^L \times \vec{D}_2^L) \cdot \hat{z}^L e^{i\omega_{12}\tau} \\
& \left. \right\} + \text{c.c.} \tag{79}
\end{aligned}$$

$$+ \left[ (\vec{D}_1^{*L} \cdot \hat{x}^L)(\vec{D}_2^L \cdot \hat{x}^L) + (\vec{D}_1^{*L} \cdot \hat{y}^L)(\vec{D}_2^L \cdot \hat{y}^L) \right] i\sigma (\vec{d}_1^L \times \vec{d}_2^L) \cdot \hat{z}^L e^{i\omega_{12}\tau} \tag{80}$$

$$+ \left[ (\vec{d}_1^L \cdot \hat{x}^L)(\vec{D}_2^L \cdot \hat{x}^L) + (\vec{d}_1^L \cdot \hat{y}^L)(\vec{D}_2^L \cdot \hat{y}^L) \right] i\sigma (\vec{D}_1^{*L} \times \vec{d}_2^L) \cdot \hat{z}^L e^{i\omega_{12}\tau} \tag{81}$$

$$+ \left[ (\vec{D}_1^{*L} \cdot \hat{x}^L)(\vec{d}_2^L \cdot \hat{x}^L) + (\vec{D}_1^{*L} \cdot \hat{y}^L)(\vec{d}_2^L \cdot \hat{y}^L) \right] i\sigma (\vec{d}_1^L \times \vec{D}_2^L) \cdot \hat{z}^L e^{i\omega_{12}\tau} \tag{82}$$

$$- 2\sigma^2 (\vec{d}_1^L \times \vec{d}_2^L) \cdot \hat{z}^L (\vec{D}_1^{*L} \times \vec{D}_2^L) \cdot \hat{z}^L e^{i\omega_{12}\tau} \tag{83}$$

$$- 2\sigma^2 (\vec{D}_1^{*L} \times \vec{d}_2^L) \cdot \hat{z}^L (\vec{d}_1^L \times \vec{D}_2^L) \cdot \hat{z}^L e^{i\omega_{12}\tau} \tag{84}$$

$$\left. \right\} + \text{c.c.} \tag{85}$$

$$\tag{86}$$

The yield in Eq. (78) satisfies the equation

$$W_\sigma - W_{-\sigma} = C \int d\Theta_k \left\{ \left[ (\vec{d}_1^{*L} \cdot \hat{x}^L)(\vec{d}_2^L \cdot \hat{x}^L) + (\vec{d}_1^{*L} \cdot \hat{y}^L)(\vec{d}_2^L \cdot \hat{y}^L) \right] i\sigma(\vec{D}_1^{*L} \times \vec{D}_2^L) \cdot \hat{z}^L e^{i\omega_{12}\tau} \right. \quad (87)$$

$$\left. + \left[ (\vec{D}_1^{*L} \cdot \hat{x}^L)(\vec{D}_2^L \cdot \hat{x}^L) + (\vec{D}_1^{*L} \cdot \hat{y}^L)(\vec{D}_2^L \cdot \hat{y}^L) \right] i\sigma(\vec{d}_1^{*L} \times \vec{d}_2^L) \cdot \hat{z}^L e^{i\omega_{12}\tau} \right. \quad (88)$$

$$\left. + \left[ (\vec{d}_2^{*L} \cdot \hat{x}^L)(\vec{D}_1^L \cdot \hat{x}^L) + (\vec{d}_2^{*L} \cdot \hat{y}^L)(\vec{D}_1^L \cdot \hat{y}^L) \right] i\sigma(\vec{D}_2^{*L} \times \vec{d}_1^L) \cdot \hat{z}^L e^{i\omega_{12}\tau} \right. \quad (89)$$

$$\left. + \left[ (\vec{D}_2^{*L} \cdot \hat{x}^L)(\vec{d}_1^L \cdot \hat{x}^L) + (\vec{D}_2^{*L} \cdot \hat{y}^L)(\vec{d}_1^L \cdot \hat{y}^L) \right] i\sigma(\vec{d}_2^{*L} \times \vec{D}_1^L) \cdot \hat{z}^L e^{i\omega_{12}\tau} \right. \quad (90)$$

On the other hand we have

$$\sigma\Omega_\sigma^L(\rho) \cdot \hat{z}^L - (-\sigma)\Omega_{-\sigma}^L(\rho) \cdot \hat{z}^L = C \int d\Theta_k \left\{ \right. \quad (91)$$

$$\left. + \left[ (\vec{d}_1^L \cdot \hat{x}^L)(\vec{d}_2^L \cdot \hat{x}^L) + (\vec{d}_1^L \cdot \hat{y}^L)(\vec{d}_2^L \cdot \hat{y}^L) \right] i\sigma(\vec{D}_1^{*L} \times \vec{D}_2^L) \cdot \hat{z}^L e^{i\omega_{12}\tau} \right. \quad (91)$$

$$\left. + \left[ (\vec{D}_1^{*L} \cdot \hat{x}^L)(\vec{D}_2^L \cdot \hat{x}^L) + (\vec{D}_1^{*L} \cdot \hat{y}^L)(\vec{D}_2^L \cdot \hat{y}^L) \right] i\sigma(\vec{d}_1^{*L} \times \vec{d}_2^L) \cdot \hat{z}^L e^{i\omega_{12}\tau} \right. \quad (92)$$

$$\left. + \left[ (\vec{d}_1^L \cdot \hat{x}^L)(\vec{D}_2^L \cdot \hat{x}^L) + (\vec{d}_1^L \cdot \hat{y}^L)(\vec{D}_2^L \cdot \hat{y}^L) \right] i\sigma(\vec{D}_1^{*L} \times \vec{d}_2^L) \cdot \hat{z}^L e^{i\omega_{12}\tau} \right. \quad (93)$$

$$\left. + \left[ (\vec{D}_1^{*L} \cdot \hat{x}^L)(\vec{d}_2^L \cdot \hat{x}^L) + (\vec{D}_1^{*L} \cdot \hat{y}^L)(\vec{d}_2^L \cdot \hat{y}^L) \right] i\sigma(\vec{d}_1^{*L} \times \vec{D}_2^L) \cdot \hat{z}^L e^{i\omega_{12}\tau} \right. \quad (94)$$

$$\left. \right\} + \text{c.c.}, \quad (95)$$

such that

$$W_\sigma - W_{-\sigma} = C\sigma\Omega_\sigma^L(\rho) \cdot \hat{z}^L - (-\sigma)\Omega_{-\sigma}^L(\rho) \cdot \hat{z}^L \quad (96)$$

$$= \sigma(\Omega_\sigma^L(\rho) + \Omega_{-\sigma}^L(\rho)) \cdot \hat{z}^L. \quad (97)$$

## Appendix F: Berry curvature for circular pump and probe fields

The wave function expressed in first order perturbation theory is

$$|\psi\rangle = |0\rangle + i \sum_j \vec{d}_j \cdot \vec{E}_j |k\rangle - \sum_j \int d\Theta_k (\vec{D}_j \cdot \vec{E}_{kj}) (\vec{d}_j \cdot \vec{E}_j) e^{-i\omega_j\tau} |\vec{k}\rangle. \quad (98)$$

The corresponding curvature is

$$\Omega = i \langle \nabla_E \psi | \times | \nabla_E \psi \rangle \quad (99)$$

$$|\nabla_E \Psi\rangle = i \sum_j |E_{\omega_j}\rangle |\vec{d}_j\rangle |k\rangle - \sum_j |E_{\omega_j}\rangle |E_{\omega_{k_j}}\rangle \int d\Theta_k \left[ \vec{D}_j (\vec{d}_j \cdot \vec{E}_j) + (\vec{D}_j \cdot \vec{E}_{k_j}) \vec{d}_j \right] e^{-i\omega_j \tau} |\vec{k}\rangle \quad (100)$$

Using the orthogonality of the basis, we get

$$\begin{aligned} -i\vec{\Omega} &= \sum_j |E_{\omega_j}\rangle |\vec{d}_j^* \times \vec{d}_j\rangle \\ &+ \sum_{jl} |E_{\omega_j}\rangle |E_{\omega_{k_j}}\rangle |E_{\omega_l}\rangle |E_{\omega_{kl}}\rangle \int d\Theta_k \left[ \vec{D}_j^* (\vec{d}_j \cdot \vec{E}_j)^* + (\vec{D}_j \cdot \vec{E}_{k_j})^* \vec{d}_j^* \right] \times \left[ \vec{D}_l (\vec{d}_l \cdot \vec{E}_l) + (\vec{D}_l \cdot \vec{E}_{kl}) \vec{d}_l \right] e^{i\omega_{jl} \tau} \end{aligned} \quad (101)$$

Since the dipole moments  $\vec{d}_l$  are real the connection simplifies to

$$-i\vec{\Omega} = \sum_{jl} |E_{\omega_j}\rangle |E_{\omega_{k_j}}\rangle |E_{\omega_l}\rangle |E_{\omega_{kl}}\rangle \int d\Theta_k \left[ \vec{D}_j^* (\vec{d}_j \cdot \vec{E}_j^*) + (\vec{D}_j \cdot \vec{E}_{k_j})^* \vec{d}_j \right] \times \left[ \vec{D}_l (\vec{d}_l \cdot \vec{E}_l) + (\vec{D}_l \cdot \vec{E}_{kl}) \vec{d}_l \right] e^{i\omega_{jl} \tau} \quad (102)$$

We employ the identity

$$\int d\Theta_k \vec{D}_j \times \vec{D}_j^* = 0, \quad (103)$$

such that terms satisfying  $j = l$  vanish,

$$\begin{aligned} -i\vec{\Omega} &= \sum_{j \neq l} |E_{\omega_j}\rangle |E_{\omega_{k_j}}\rangle |E_{\omega_l}\rangle |E_{\omega_{kl}}\rangle \int d\Theta_k \left[ (\vec{d}_j \cdot \vec{E}_j^*) (\vec{d}_l \cdot \vec{E}_l) (\vec{D}_j^* \times \vec{D}_l) \right. \\ &\quad + (\vec{d}_j \cdot \vec{E}_j^*) (\vec{D}_l \cdot \vec{E}_{kl}) (\vec{D}_j^* \times \vec{d}_l) \\ &\quad + (\vec{D}_j \cdot \vec{E}_{k_j})^* (\vec{d}_l \cdot \vec{E}_l) (\vec{d}_j \times \vec{D}_l) \\ &\quad \left. + (\vec{D}_j \cdot \vec{E}_{k_j})^* (\vec{D}_l \cdot \vec{E}_{kl}) (\vec{d}_j \times \vec{d}_l) \right] e^{i\omega_{jl} \tau}. \end{aligned} \quad (104)$$

Due to the anti-symmetry of the cross product, the curvature can be expressed as

$$\begin{aligned} \vec{\Omega} = -2C \int d\Theta_k \left[ \text{Im} \left\{ (\vec{d}_1 \cdot \vec{E}_1^*) (\vec{d}_2 \cdot \vec{E}_2) (\vec{D}_1^* \times \vec{D}_2) e^{i\omega_{12}\tau} \right\} \right. \\ + \text{Im} \left\{ (\vec{d}_1 \cdot \vec{E}_1^*) (\vec{D}_2 \cdot \vec{E}_{k2}) (\vec{D}_1^* \times \vec{d}_2) e^{i\omega_{12}\tau} \right\} \\ + \text{Im} \left\{ (\vec{D}_1 \cdot \vec{E}_{k1})^* (\vec{d}_2 \cdot \vec{E}_2) (\vec{d}_1 \times \vec{D}_2) e^{i\omega_{12}\tau} \right\} \\ \left. + \text{Im} \left\{ (\vec{D}_1 \cdot \vec{E}_{k1})^* (\vec{D}_2 \cdot \vec{E}_{k2}) (\vec{d}_1 \times \vec{d}_2) e^{i\omega_{12}\tau} \right\} \right], \end{aligned} \quad (105)$$

where we defined

$$C = |E_{\omega_1}| |E_{\omega_{k1}}| |E_{\omega_2}| |E_{\omega_{k2}}|. \quad (106)$$

- 
- [1] D. Ayuso, O. Neufeld, A. F. Ordonez, P. Decleva, G. Lerner, O. Cohen, M. Ivanov, and O. Smirnova, Synthetic chiral light for efficient control of chiral light-matter interaction, *Nature Photonics* **13**, 866 (2019).
- [2] D. Ayuso, A. F. Ordonez, and O. Smirnova, Ultrafast chirality: the road to efficient chiral measurements, *PCCP* **24**, 26962 (2022).
- [3] P. Král and M. Shapiro, Cyclic population transfer in quantum systems with broken symmetry, *Physical Review Letters* **87**, 183002 (2001).
- [4] S. Eibenberger, J. Doyle, and D. Patterson, Enantiomer-specific state transfer of chiral molecules, *Phys. Rev. Lett.* **118**, 123002 (2017).
- [5] C. Pérez, A. L. Steber, S. R. Domingos, A. Krin, D. Schmitz, and M. Schnell, Coherent enantiomer-selective population enrichment using tailored microwave fields, *Angewandte Chemie International Edition* **56**, 12512 (2017), <https://onlinelibrary.wiley.com/doi/pdf/10.1002/anie.201704901>.
- [6] A. Ordóñez, P. Vindel-Zandbergen, and D. Ayuso, Chiral coherent control of electronic population transfer: towards all-optical and highly enantioselective photochemistry (2023), [arXiv:2309.02392 \[physics.chem-ph\]](https://arxiv.org/abs/2309.02392).
- [7] C. Ye, Y. Sun, L. Fu, and X. Zhang, Phase-matched locally chiral light for global control of chiral light-matter interaction, *Opt. Lett.* **48**, 5511 (2023).
- [8] D. Ayuso, A. F. Ordonez, P. Decleva, M. Ivanov, and O. Smirnova, Enantio-sensitive unidirectional light bending, *Nature Communications* **12**, 3951 (2021).

- [9] M. Khokhlova, E. Pisanty, S. Patchkovskii, O. Smirnova, and M. Ivanov, Enantiosensitive steering of free-induction decay, *Science Advances* **8**, eabq1962 (2022), <https://www.science.org/doi/pdf/10.1126/sciadv.abq1962>.
- [10] N. Mayer, D. Ayuso, P. Decleva, M. Khokhlova, E. Pisanty, M. Ivanov, and O. Smirnova, arxiv:2303.10932 (2023).
- [11] S. Beaulieu, A. Comby, D. Descamps, B. Fabre, G. A. Garcia, R. Géneaux, A. G. Harvey, F. Légaré, Z. Mašín, L. Nahon, A. F. Ordonez, S. Petit, B. Pons, Y. Mairesse, O. Smirnova, and V. Blanchet, Photoexcitation circular dichroism in chiral molecules, *Nature Physics* **14**, 484 (2018).
- [12] C. A. Mead, The geometric phase in molecular systems, *Reviews of modern physics* **64**, 51 (1992).
- [13] A. F. Ordonez and O. Smirnova, Propensity rules in photoelectron circular dichroism in chiral molecules. II. General picture, *Physical Review A* **99**, 043417 (2019).
- [14] K. Schwennicke and J. Yuen-Zhou, Enantioselective topological frequency conversion, *The Journal of Physical Chemistry Letters* **13**, 2434 (2022).
- [15] J. S. Peter, S. Ostermann, and S. F. Yelin, Chirality-induced emergent spin-orbit coupling in topological atomic lattices, arXiv preprint arXiv:2311.09303 (2023).
- [16] A. F. Ordonez, D. Ayuso, P. Decleva, and O. Smirnova, Geometric magnetism and anomalous enantiosensitive observables in photoionization of chiral molecules, *Communications Physics* **6**, 257 (2023).
- [17] J. Leinaas and J. Myrheim, On the theory of identical particles, *Il nuovo cimento* **37**, 132 (1977).
- [18] C. L. Kane and E. J. Mele, Quantum spin hall effect in graphene, *Physical review letters* **95**, 226801 (2005).
- [19] B. A. Bernevig, T. L. Hughes, and S.-C. Zhang, Quantum spin hall effect and topological phase transition in hgte quantum wells, *science* **314**, 1757 (2006).
- [20] C. Nayak, S. H. Simon, A. Stern, M. Freedman, and S. D. Sarma, Non-abelian anyons and topological quantum computation, *Reviews of Modern Physics* **80**, 1083 (2008).
- [21] C. Cisowski, J. Götze, and S. Franke-Arnold, Colloquium: Geometric phases of light: Insights from fiber bundle theory, *Reviews of Modern Physics* **94**, 031001 (2022).
- [22] T. Ozawa, H. M. Price, A. Amo, N. Goldman, M. Hafezi, L. Lu, M. C. Rechtsman, D. Schuster, J. Simon, O. Zilberberg, and I. Carusotto, Topological photonics, *Rev. Mod. Phys.* **91**, 015006 (2019).
- [23] R. Weinkauff, E. Schlag, T. Martinez, and R. Levine, Nonstationary electronic states and site-selective reactivity, *The Journal of Physical Chemistry A* **101**, 7702 (1997).
- [24] L. Cederbaum and J. Zobeley, Ultrafast charge migration by electron correlation, *Chemical Physics Letters* **307**, 205 (1999).

- [25] J. Breidbach and L. S. Cederbaum, Migration of holes: Formalism, mechanisms, and illustrative applications, *JCP* **118**, 3983 (2003).
- [26] F. Remacle and R. D. Levine, An electronic time scale in chemistry, *Proceedings of the National Academy of Sciences* **103**, 6793 (2006), <https://www.pnas.org/content/103/18/6793.full.pdf>.
- [27] A. I. Kuleff and L. S. Cederbaum, Ultrafast correlation-driven electron dynamics, *Journal of Physics B: Atomic, Molecular and Optical Physics* **47**, 124002 (2014).
- [28] F. Calegari, D. Ayuso, A. Trabattoni, L. Belshaw, S. De Camillis, S. Anumula, F. Frassetto, L. Poletto, A. Palacios, P. Decleva, J. B. Greenwood, F. Martín, and M. Nisoli, Ultrafast electron dynamics in phenylalanine initiated by attosecond pulses, *Science* **346**, 336 (2014), <https://science.sciencemag.org/content/346/6207/336.full.pdf>.
- [29] M. Nisoli, P. Decleva, F. Calegari, A. Palacios, and F. Martín, Attosecond electron dynamics in molecules, *Chemical Reviews* **117**, 10760 (2017), PMID: 28488433.
- [30] J. Delgado, M. Lara-Astiaso, J. González-Vázquez, P. Decleva, A. Palacios, and F. Martín, Molecular fragmentation as a way to reveal early electron dynamics induced by attosecond pulses, *Faraday Discuss.* **228**, 349 (2021).
- [31] Y. Aharonov and J. Anandan, Phase change during a cyclic quantum evolution, *Phys. Rev. Lett.* **58**, 1593 (1987).
- [32] S. Beaulieu, A. Comby, D. Descamps, B. Fabre, G. A. Garcia, R. Géneaux, A. G. Harvey, F. Légaré, Z. Mašín, L. Nahon, A. F. Ordonez, S. Petit, B. Pons, Y. Mairesse, O. Smirnova, and V. Blanchet, Photoexcitation circular dichroism in chiral molecules, *Nature Physics* **14**, 484 (2018).
- [33] V. Wanie, E. Bloch, E. P. Månsson, L. Colaizzi, S. Ryabchuk, K. Saraswathula, A. F. Ordonez, D. Ayuso, O. Smirnova, A. Trabattoni, *et al.*, Capturing electron-driven chiral dynamics in uv-excited molecules, *Nature* , 1 (2024).